Late-transition versus smooth $H(z)$-deformation models for the resolution of the Hubble crisis

George Alestas,[1,*] David Camarena,[2,†] Eleonora Di Valentino,[3,‡] Lavrentios Kazantzidis,[1,§] Valerio Marra,[4,5,6,‖] Savvas Nesseris,[7,¶] and Leandros Perivolaropoulos[1,**]

[1]*Department of Physics, University of Ioannina, GR-45110 Ioannina, Greece*
[2]*PPGCosmo, Universidade Federal do Espírito Santo, 29075-910 Vitória, ES, Brazil*
[3]*School of Mathematics and Statistics, University of Sheffield, Hounsfield Road, Sheffield S3 7RH, United Kingdom*
[4]*Núcleo de Astrofísica e Cosmologia and Departamento de Física, Universidade Federal do Espírito Santo, 29075-910 Vitória, ES, Brazil*
[5]*INAF-Osservatorio Astronomico di Trieste, via Tiepolo 11, Trieste 34131, Italy*
[6]*IFPU-Institute for Fundamental Physics of the Universe, via Beirut 2, Trieste 34151, Italy*
[7]*Instituto de Física Teórica UAM-CSIC, Universidad Autonóma de Madrid, Cantoblanco, Madrid 28049, Spain*

(Received 19 October 2021; accepted 25 February 2022; published 29 March 2022)

Gravitational transitions at low redshifts ($z_t < 0.1$) have been recently proposed as a solution to the Hubble and growth tensions. Such transitions would naturally lead to a transition in the absolute magnitude M of type Ia supernovae (SNIa) at z_t (late M transitions—*LMT*) and possibly in the dark energy equation of state parameter w (late $w-M$ transitions). Here, we compare the quality of fit of this class of models to cosmological data, with the corresponding quality of fit of the cosmological constant model (ΛCDM) and some of the best smooth $H(z)$ deformation models [wCDM (cold dark matter), Chevallier-Polarski-Linder, phenomenologically emergent dark energy]. We also perform model selection via the Akaike information criterion (AIC) and the Bayes factor. We use the full cosmic microwave background temperature anisotropy spectrum data, the baryon acoustic oscillations data, the Pantheon SNIa data, the SNIa absolute magnitude M as determined by Cepheid calibrators and the value of the Hubble constant H_0 as determined by local SNIa calibrated using Cepheids. We find that smooth $H(z)$ deformation models perform worse than transition models for the following reasons: (1) they have a worse fit to low-z geometric probes (baryon acoustic oscillations and SNIa data); (2) they favor values of the SNIa absolute magnitude M that are lower as compared to the value M_c obtained with local Cepheid calibrators at $z < 0.01$; (3) They tend to worsen the $\Omega_{m,0} - \sigma_{8,0}$ growth tension. We also find that the $w-M$ transition model does not provide a better quality of fit to cosmological data than a pure M transition model (*LMT*), where w is fixed to the ΛCDM value $w = -1$ at all redshifts. We conclude that the *LMT* model has significant statistical advantages over smooth late-time $H(z)$ deformation models in addressing the Hubble crisis.

DOI: 10.1103/PhysRevD.105.063538

I. INTRODUCTION

The scenario considered as the standard model in cosmology is the cosmological constant Λ and cold dark matter (CDM) model, hereafter denoted as ΛCDM, as it is remarkably successful in fitting cosmological and astrophysical observations on a vast range of scales. However, this scenario is not a first principles theory, and it is based on unknown quantities (dark matter, dark energy and inflation), therefore can be considered as a low energy and large scales approximation to a physical law, which has yet to be discovered. In this context, the observational problems in the estimates of the main cosmological parameters, see Refs. [1–4], can hint towards the presence of deviations from the ΛCDM scenario [5,6].

In particular, the most statistically significant inconsistency is the well known Hubble constant H_0 *tension*, currently above the 4σ level (see [5,7–11] and references therein). This tension refers to the disagreement between the value of H_0 estimated from the Planck satellite data [12], assuming a ΛCDM model, and the H_0 measured by the SH0ES collaboration [13]. However, there are many ways to obtain the Hubble constant value, and most of the

*g.alestas@uoi.gr
†david.f.torres@aluno.ufes.br
‡e.divalentino@sheffield.ac.uk
§l.kazantzidis@uoi.gr
‖valerio.marra@me.com
¶savvas.nesseris@csic.es
**leandros@uoi.gr

early indirect estimates agree with Planck, as the cosmic microwave background (CMB) ground telescopes [14,15] or the baryon acoustic oscillations (BAO) measurements [16], while most of the late time measurements agree with SH0ES, even if obtained with different teams, methods or geometric calibrators [17–21]. Finally, there are a few measurements that are in agreement with both sides, as the tip of the red giant branch [22], even if the reanalysis of [23] shows a better consistency with the SH0ES value, or those based on the time delay [24].

An additional challenge for the standard model is the *growth tension*. Dynamical cosmological probes favor weaker growth of perturbations than geometric probes in the context of general relativity and the $Planck18/\Lambda$CDM standard model at a level of about 3σ [25–31]. It would therefore be of particular interest to construct theoretical models that have the potential to simultaneously address both the H_0 and growth tensions.

A wide range of theoretical models have been proposed as possible resolutions of the Hubble tension [10,30]. They can be divided in three broad classes:

(i) "Early time" models that recalibrate the scale of the sound horizon at recombination by modifying physics during the prerecombination epoch. These models deform the Hubble expansion rate before recombination at $z > 1100$ by introducing early dark energy [32–53], extra neutrinos or relativistic species at recombination [54–75], features in the primordial power spectrum [76,77] or evaporating primordial black holes [78] etc. These models however, can alleviate but not fully solve the Hubble tension [79–81], and they tend to predict stronger growth of perturbations than implied by dynamical probes like redshift space distortion (RSD) and weak lensing data and thus they worsen the growth tension [82]. This issue however is still under debate [83].

(ii) Late time deformations of the Hubble expansion rate $H(z)$ that assume a deformation of the best fit $Planck18/\Lambda$CDM $H(z)$ at late times. With the term "deformation" we refer to a modification of the Planck/ΛCDM best fit form of $H(z)$ such that the new form of $H(z)$ not only tends to satisfy the local measurements of H_0 instead of the CMB best fit value, but also leads to an angular scale of the sound horizon that is consistent with the observed CMB peaks. The analytical method for the construction of such "deformed" $H(z)$ is described in Ref. [84]. In this context, $H(z)$ retains its consistency with the observed CMB anisotropy spectrum while reaching the locally measured value of $H(z = 0)$. In this class of models we can find both interacting dark matter [85–90] or dark energy cosmologies [9,71,91–113], or extended and exotic dark energy models [54,114–148]. While the interacting dark energy models need further investigations,[1] smooth $H(z)$ deformations due to the extended dark energy cosmologies have difficulty in fitting low z cosmological distance measurements obtained by BAO and SNIa data [150]. In addition, this class of models tends to imply a lower value of SNIa absolute magnitude M than the value implied by Cepheid calibrators [151]. Thus, this class of models cannot fully resolve the Hubble problem [123,152–154], as demonstrated also in the present analysis for a few extended dark energy cosmologies.

(iii) Late time transitions at a redshift $z_t \lesssim 0.01$ of the SNIa absolute magnitude M have also been proposed as possible models that have the potential to resolve the Hubble tension [84,155]. These models assume an abrupt transition of M to a lower value (brighter SNIa at $z > z_t$) by $\Delta M \simeq -0.2$ mag. Such a reduction of M could have been induced by a fundamental physics transition of the effective gravitational constant $G_{\rm eff}$. This type of transition[2] could coexist with a transition of the dark energy equation of state w from $w = -1$ at $z > z_t$ to a lower value at $z < z_t$ (phantom transition). This class of models could fully resolve the Hubble problem while at the same time address the growth tension by reducing the growth rate of cosmological perturbation due to the lower value of $G_{\rm eff}$ at $z > z_t$ [155]. Such models are highly predictive and have been challenged by existing, see Ref. [157], and upcoming (e.g. Gravitational Waves Standard Sirens and Tully-Fisher data [160]) cosmological and astrophysical [161] data. Observationally, viable theoretical models that can support this transition include scalar-tensor theories with potentials where a first order late phase transition takes place [159,162,163].

Most previous studies usually marginalize over the SNIa absolute magnitude, treating it as a nuisance parameter [164–167]. In particular, they consider the M-independent $\tilde{\chi}^2 \equiv -2 \log \int dM \exp(-\chi^2/2)$ function instead of the full χ^2 function which explicitly depends on M. In our analysis the parameter M is not marginalized over and is included in the Monte Carlo Markov chain (MCMC) exploration along with the cosmological parameters. This allows us to compare our results with the corresponding inverse distance ladder constraints of [168,169], even though in the context of SNIa data its degeneracy with H_0 is acknowledged. However, in Refs. [168,169] the case of a transition in M is not considered and this is one important difference

[1]See, for example, Ref. [149] for a study of the Interacting Dark Energy models with SNIa data.

[2]A possible evolution of the absolute magnitude M has also been recently investigated in Refs. [156–159].

from our approach along with the types of data considered in the fit. Thus, in view of the latter class of models, the designation M tension/crisis might be more suitable to describe the problem [170,171]. At its core, the issue is due to the fact that the supernova absolute magnitude M used to derive the local H_0 constraint by the SH0ES collaboration is at a mismatch with the value of M that is necessary to fit SNIa, CMB and BAO data.

Note that the local distance ladder methodology of SH0ES considers SNIa data in the redshift range of $0.023 < z < 0.15$. This makes the overall method oblivious to any transitions in the value of M at very low redshifts [84]. In particular, the distance ladder methodology makes the crucial assumption that M is the same at all redshifts. If this assumption is withdrawn and a transition is allowed at $z < 0.01$ then the inferred value of H_0 may change significantly. For example if the transition occurs at $z = 0.01$ then the calibrated value of M correctly obtained at $z < 0.01$ will not be the same as the value of M at $z > 0.01$ even though the value is assumed to be the same in the distance ladder methodology. Also, if the M transition takes place at $z < 0.01$ and the calibration analysis does not allow for such a transition then an incorrect value for M will be obtained by the calibration analysis [172]. Since in the Hubble flow ($z > 0.01$), the SNIa absolute magnitude M is degenerate with H_0 through the observable $\mathcal{M} = M - 5\log_{10}(h) + 42.38$, where $h = H_0/100\ \mathrm{km\,s^{-1}\,Mpc^{-1}}$, it becomes clear that if the true value of M in the Hubble flow was lower than the value of M for $z < 0.01$ then correspondingly the true value of H_0 would also be lower and would become consistent with the CMB inferred value. If the transition occurs at $z < 0.01$, SNIa in the Hubble flow $(0.023 < z < 0.15)$ will naturally follow the calibration provided by CMB + BAO leading to a lower value on the Hubble constant.

Hints for such a late time transition may be seen in a recent reanalysis of the Cepheid SNIa calibration data where the Cepheid color-luminosity parameter is allowed to vary among galaxies [172,173]. More specifically, in Refs. [172,173] hints were found for a transition of this parameter or at least for it having a different value for the anchor galaxies compared to the SNIa host galaxies. Even though the errors of the individual R_E parameters for each host are consistent with the corresponding anchor (low distance) values (see Figs. 4 and 5 of Ref. [173]), when binning is implemented, the hints for a consistently different value (transition) becomes statistically more significant as shown in Ref. [172]. It is important to note here that the binning performed in Ref. [172] is not an anchor-calibrator binning, but one based on distance (low distance bin vs high distance bin separated by a critical distance D_c). The latter type of binning is justified and in this case led to a 2σ difference regarding the best fit values of R_W and M_W between the low distance bin and the high distance bin, at $D_c \approx 18$ Mpc. This 2σ level of mismatch is clearly not statistically significant enough, but it is of interest to consider that if this degree of freedom is allowed (different values of R_W and/or M_W between high and low distance bins) the favored value of the best fit Hubble parameter becomes consistent with the CMB inferred value. This issue however is currently under debate and needs to be carefully interpreted.

In the present analysis we focus on late time M transition models (LMT), possibly featuring also a transition in the dark energy equation of state parameter w ($LwMT$), and compare their quality of fit to cosmological data with $H(z)$ deformation models. In particular, we address the following questions:

(i) How much does the quality of fit to low-z cosmological data improve for LMT models as compared to smooth $H(z)$ deformation models?
(ii) What is the level of M transition favored by data?
(iii) What is the value of M favored by smooth $H(z)$ deformation models and how does it compare with the value of M favored by Cepheid calibrators?
(iv) Does the addition of a w transition on top of the M transition significantly improve the quality of fit to the data?

Previous studies [84,151,155] have indicated that LMT models have improved quality of fit to cosmological data. However, those studies did not make use of the full CMB anisotropy spectrum but only effective parameters (shift parameter). The present analysis improves on those studies by implementing a more complete and accurate approach using the full *Planck18* CMB anisotropy spectrum in the context of a Boltzmann code and a MCMC analysis.

The structure of our paper is the following: in the next Sec. II we focus on transition models ($LwMT$ and LMT) and present the constraints on their parameters using up-to-date cosmological data. In Sec. III we compare the quality of fit to cosmological data of transition models with the corresponding quality of fit of $H(z)$ deformation models; we also perform model selection. Finally, in Sec. IV we summarize our results, discuss possible interpretations and present possible extensions of the present analysis.

II. TRANSITION MODELS CONFRONTED BY OBSERVATIONAL DATA

The LMT model includes a sharp transition in the SNIa absolute magnitude M of the form

$$M(z) = M_< + \Delta M \Theta(z - z_t), \tag{2.1}$$

where z_t is the transition redshift, $M_< \equiv M_c = -19.24$ mag is the local Cepheid-calibrated value from SH0ES as reconstructed in Refs. [170,174] (in this section we neglect uncertainties on M_c), ΔM is the parameter that quantifies the shift from the M_c value, and Θ is the Heaviside step function. The $LwMT$ was first introduced in Ref. [84] and

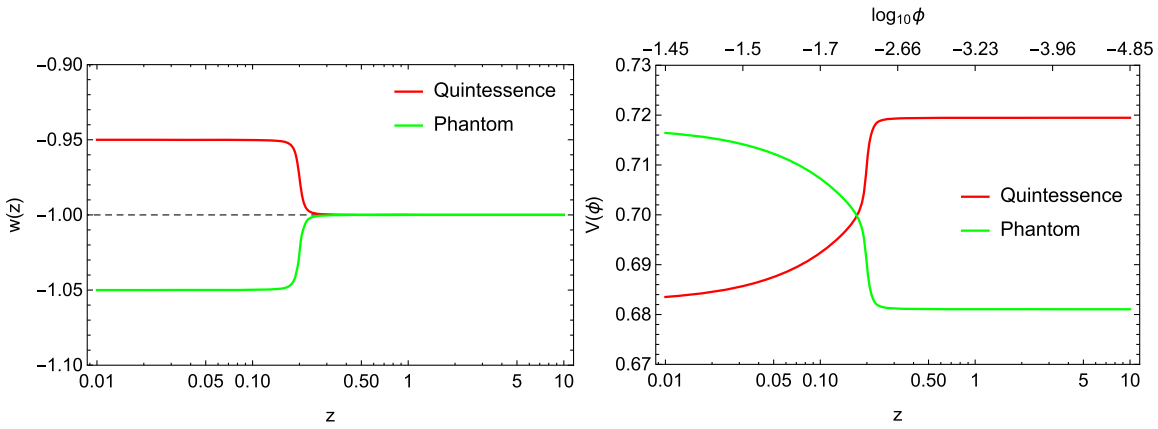

FIG. 1. An example of a transition in the dark energy equation of state w (left panel) and how it can be caused by a sharp transition in a quintessence (red line) or phantom (green line) potential (right panel), with the scalar field running down/up the potential, respectively. Here we assumed a smooth transition and reconstructed the potentials following Ref. [175], assuming $\Omega_{\mathrm{m},0} = 0.3$, $z_t = 0.2$, $\Delta w = \pm 0.05$ for quintessence/phantom fields.

has, in addition to the M transition, a dark energy equation of state w transition of the form

$$w(z) = -1 + \Delta w \Theta(z_t - z), \tag{2.2}$$

where Δw describes the shift from the ΛCDM value $(w = -1)$ for $z < z_t$. Both Δw and ΔM are parameters to be determined by the data.

Such transitions in the dark energy equation of state $w(z)$ are in principle well motivated and can easily happen within the context of a minimally coupled scalar field in general relativity, either of the quintessence or phantom type. For example, in Fig. 1 we show a transition in the dark energy equation of state w (left panel) and how it can be caused by a sharp transition in a quintessence (red line) or phantom (green line) potential (right panel), with the scalar field running down/up the potential, respectively. For this plot we assumed, as an example, a smooth transition and reconstructed the potentials following the procedure of Ref. [175], assuming $\Omega_{\mathrm{m},0} = 0.3$, $z_t = 0.2$, $\Delta w = \pm 0.05$ for quintessence $(+)$ and phantom $(-)$ fields. By adjusting the aforementioned parameters, one may tune both the steepness and the redshift of the transition.

In order to constrain these transition models we use the following data combination:

(i) The *Planck18* temperature CMB data, including the TTTEEE likelihoods for high-l ($l > 30$), the temperature data TT and EE power spectra data for low-l ($2 < l < 30$) [176,177], as well as the CMB lensing likelihood [178].
(ii) The BAO data presented in Refs. [179–181] as well as the Lyα BAO data of Refs. [182,183].
(iii) The latest SNIa dataset (Pantheon) presented in Ref. [184].
(iv) A robust RSD compilation discussed in Ref. [185], using the likelihood presented in Ref. [186].

To analyze the data and obtain the best fit parameters we modify the publicly available CLASS code[3] and perform the MCMC analysis using the publicly available MontePython code [187–189].

These models by construction provide a great amount of flexibility in fitting the observational data since they can mimic ΛCDM for $z > z_t$, while being fully consistent with local measurements of M. In the case of the transition occurring at very low redshifts where there are almost no available data, i.e. at $z_t < 0.01$, we would normally anticipate a fit even better to that of ΛCDM due to the extra parameter Δw in the context of $LwMT$. However, then there would be no H_0 tension, since the local measurement of H_0 should coincide with the measurement of Planck if the M transition is taken into account (a shift of M implies a shift of H_0 since the two parameters are degenerate).

Interestingly there are some works that use data with $z < 0.01$, such as the extended Pantheon dataset of the latest SH0ES analysis (Panteon+) [190] as well as the analyses of Refs. [172,191], that can be used to search self-consistently for a transition in M at $z < 0.01$ using the combined Cepheid and SNIa data. Regarding the Pantheon + dataset however, not only the data are not publicly available yet but also in our analysis we are simultaneously marginalizing over M and H_0. We also stress that we are not including the full covariance between calibrators and supernovae as in the latest SH0ES analysis. Regarding Ref. [191], the analysis makes no attempt to investigate an M transition or to constrain variations of $H(z)$ for $z < 0.01$ since this redshift region is not in the Hubble flow and thus it cannot be reliably constrained.

[3]For a step-by-step guide for the modifications implemented in CLASS, see this file https://cosmology.physics.uoi.gr/wp-content/uploads/2021/07/Class_Implementation-1.pdf.

TABLE I. The best-fit values and constraints at 68.3% C.L. and 95.5% C.L. of the parameters for the *LwMT* model and $z_t \geq 0.01$ (or equivalently $a_t \leq 0.99$) using the CMB + BAO + Pantheon + RSD likelihoods described above.

Parameter	Best fit	mean $\pm \sigma$	95.5% lower	95.5% upper
$\Omega_{m,0}$	0.3018	$0.3066^{+0.0064}_{-0.0065}$	0.2939	0.3196
n_s	0.9708	$0.9685^{+0.0038}_{-0.0037}$	0.9608	0.9759
H_0	68.56	$68.03^{+0.55}_{-0.58}$	66.94	69.15
$\sigma_{8,0}$	0.8141	0.8089 ± 0.0065	0.7957	0.8219
ΔM	−0.1676	-0.1698 ± 0.012	−0.1933	−0.1467
Δw	Unconstrained	Unconstrained	Unconstrained	Unconstrained
a_t	0.9856	>0.985	>0.984	>0.984
$M_> \equiv M_c + \Delta M$	−19.408	-19.410 ± 0.012	−19.433	−19.387
$-\ln \mathcal{L}_{\min}$		1917.02		
$\chi^2_{\min}$		3834		

In contrast, it demonstrates that variations of the $H(z)$ parametrization in the Hubble flow (for $z > 0.01$) do not affect the best fit value of H_0. This result could have been anticipated by the fact that (almost) all $H(z)$ parametrizations reduce to a cosmographic expansion in the range $0.01 < z < 0.1$ where the fit for H_0 is performed.

In addition, a separate analysis of Ref. [172], focusing on the Cepheid + SNIa data for $z < 0.01$, has found hints for a transition in the Cepheid absolute magnitude M_W and in the color luminosity parameter R_W which, if taken into account, make the value of absolute magnitude M of SNIa consistent with its inverse distance ladder value, thus resolving the Hubble tension.

Hence, in what follows we impose a prior of $z_t \geq 0.01$ that corresponds to $a_t \leq 0.99$, since any lower value of z_t cannot be probed via the considered Hubble flow data. Moreover, we use a prior of $\Delta w \in [-0.7, 0.7]$. The best fit values of the *LwMT* model with $z_t \geq 0.01$ are shown in Table I, while the $1\sigma - 2\sigma$ corresponding contours are shown in Fig. 2. In Table I we also include the parameter $M_> \equiv M_c + \Delta M$ that arises for $z > z_t$ with M_c corresponding to the Cepheid-calibrated value of the SNIa absolute magnitude.

From Table I, we see that the parameter a_t (or equivalently z_t) approaches the highest (lowest) value imposed by the data in order to achieve the best possible quality of fit favoring a transition at very low redshifts. Moreover, the posterior probability of a_t appears to be bimodal. The reason for this behavior may be seen e.g. in Fig. 9 of Ref. [84] or in Fig. 3 of Ref. [170] where the lowest z bin for the SNIa absolute magnitude M shows a rise that may be interpreted as a hint for a transition at $z \simeq 0.015$ (this is expressed by the first Plato peak for the likelihood of a_t at $a \simeq 0.0986$). The higher peak however occurs at $a_t = 0.99$ indicating that the minimum χ^2 for the transition redshift is at or below $z = 0.01$ (no clear hint for a transition in the Hubble flow). However, given that the data do not extend to more recent times than $a = 0.99$, the best fit is at $a_t = 0.9856$ as it is explicitly written in Table I and the higher peak at $a_t = 0.99$ can only be interpreted as a lower bound for the value a_t if the transition occurs at more recent times. We thus chose to neglect this second peak.

The timing of the transition is not particularly fine-tuned due to the fact that at very low redshifts dark energy has started to dominate in the Universe. Since at that time $\Omega_\Lambda > 0.5$, new physics could possibly emerge. Furthermore, in previous analyses by some of the authors of the current work [156,158] a tomographic analysis of the Pantheon dataset has been performed. In both of these references, it has been shown that for $z > 0.01$ the redshift binned best fit ΛCDM parameter values for the parameter M (as well as $\Omega_{m,0}$) vary around the full dataset fit value (assumed constant) by up to $\Delta M = 0.08 \pm 0.06$. This variation is significantly smaller than the variation $\Delta M \simeq 0.2$ required for the resolution of the Hubble tension (see e.g. the left panel of Fig. 1 of [158]). Most importantly, however, we observe that despite allowing for an extra degree of freedom induced by having $\Delta w \neq 0$, this parameter seems to be ignored by the data.

Since $z_t \approx 0.01$ is favored by the data, the parameter Δw becomes irrelevant due to the fact that for $z_t = 0.01$, Δw would modify the expansion rate $H(z)$ only in a region where there are no data available ($z < 0.01$). This carries the implication that a w transition is perhaps not needed in order to obtain the best quality of fit to the data.[4] We thus repeat the analysis considering only an M transition ("late M transition"), setting $\Delta w = 0$ and $a_t = 0.99$ (or equivalently $z_t = 0.01$), which is basically the maximum of the posterior of a_t for the *LwMT* model. We obtain the best fit and mean values as indicated in Table II; the contours are shown in Fig. 3.

[4]The w transition however may be required for theoretical reasons. In scalar tensor theories a gravitational transition to weaker gravity at early times may require a simultaneous transition to $w < -1$ at late times.

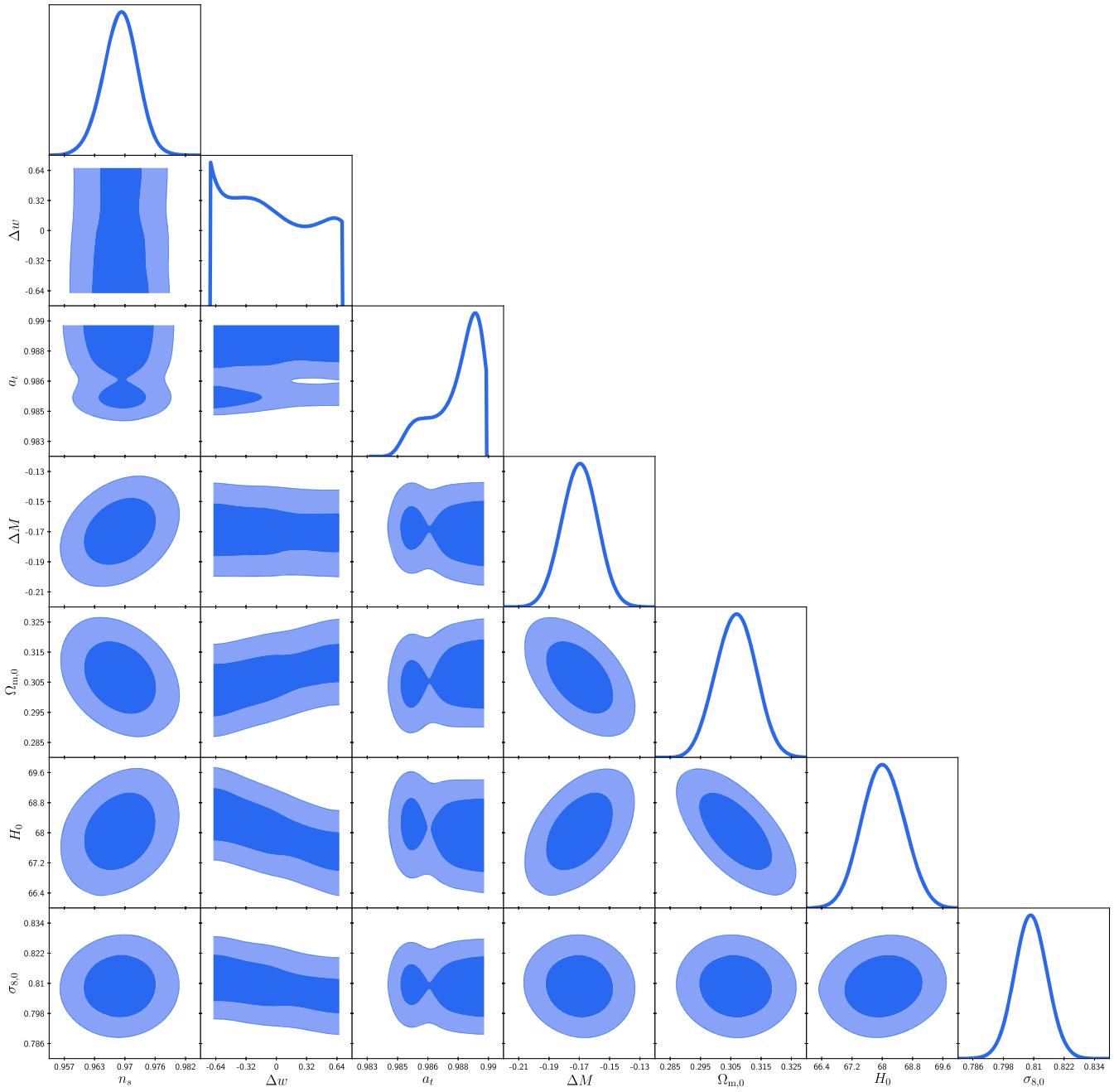

FIG. 2. The 68.3%–95.5% confidence contours for the parameters of the *LwMT* model with $z_t \geq 0.01$, using the CMB + BAO + Pantheon + RSD likelihoods.

As we can see comparing Tables I, II, and Figs. 2, 3 the introduction of Δw has practically no effect on the quality of fit, i.e. on the χ^2 value. Moreover, the mismatch between the local calibration of the SNIa absolute magnitude and the value inferred from the other probes is very significant, suggesting that the designation M tension/crisis is suitable to describe the H_0 crisis [170,171]. Finally, it is interesting to note that the inferred value of $M_> = -19.41$ mag agrees well with the constraint $M = -19.40$ mag that was obtained using the parametric-free inverse distance ladder of Ref. [192].

So, some natural questions that arise are the following: "how do the transition models *LwMT* and *LMT* compare to some other popular dark energy models in the literature that also try to address the Hubble tension?" and "can these models provide an M value that is consistent with the Cepheid measurement M_c as the transition models that we discussed?" These questions will be addressed in the following section, where we perform a comparison between some popular dark energy parametrizations (smooth deformation dark energy models) with the transition models *LwMT* and *LMT*.

TABLE II. The best-fit values and constraints at 68.3% C.L. and 95.5% C.L. of the parameters for the *LMT* model with $z_t = 0.01$ (or equivalently $a_t = 0.99$) using the CMB + BAO + Pantheon + RSD likelihoods.

Parameter	Best fit	mean $\pm\,\sigma$	95.5% lower	95.5% upper
$\Omega_{\mathrm{m},0}$	0.3088	$0.3082^{+0.0052}_{-0.0058}$	0.2976	0.3193
n_s	0.9697	$0.968^{+0.0038}_{-0.0037}$	0.9606	0.9754
H_0	67.88	$67.89^{+0.42}_{-0.40}$	67.06	68.71
$\sigma_{8,0}$	0.8085	$0.8084^{+0.0058}_{-0.0061}$	0.7963	0.8205
ΔM	−0.170	-0.172 ± 0.012	−0.195	−0.149
$M_> \equiv M_c + \Delta M$	−19.410	-19.412 ± 0.012	−19.435	−19.389
$-\ln \mathcal{L}_{\mathrm{min}}$		1917.52		
χ^2_{min}		3835		

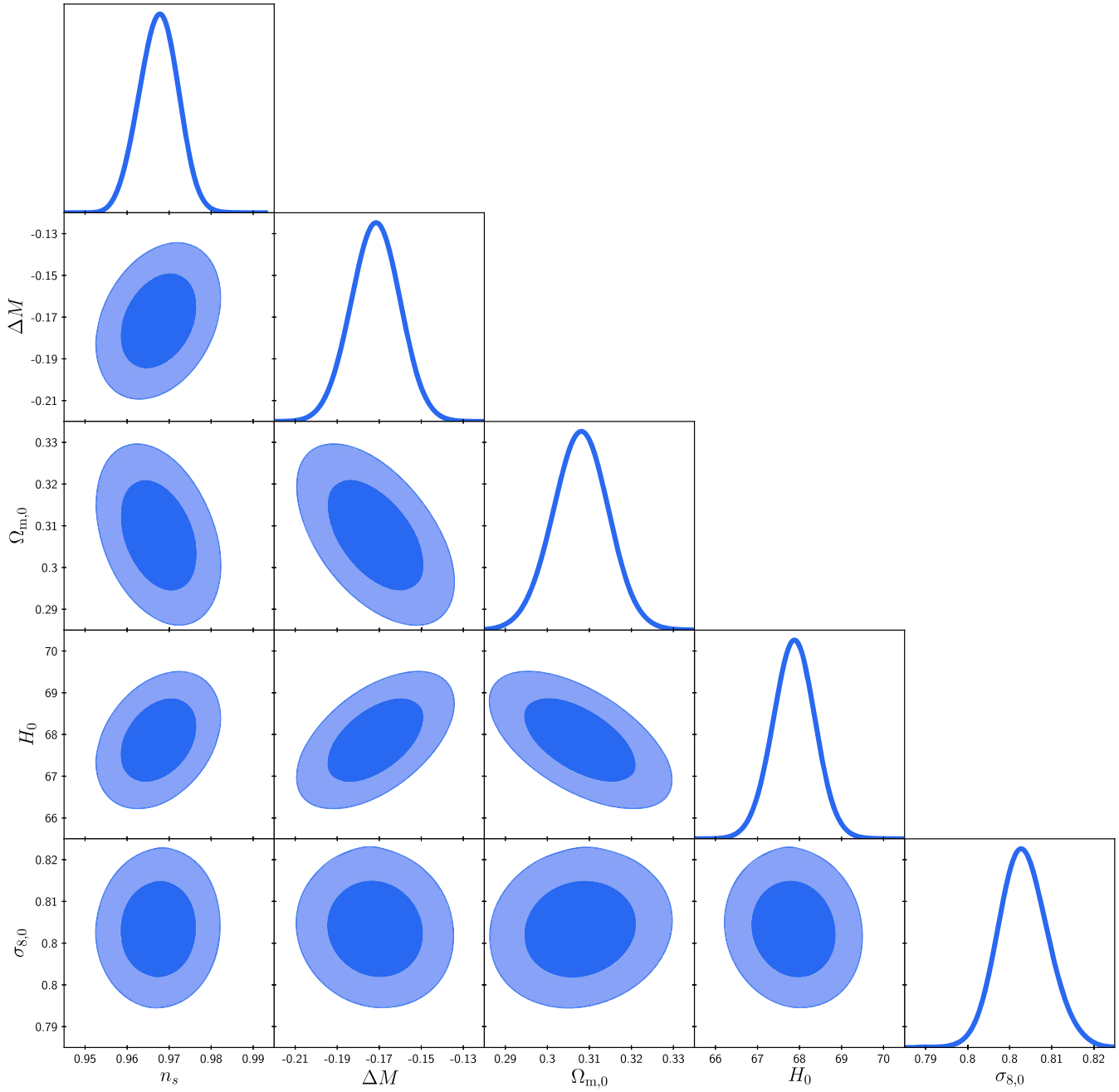

FIG. 3. The 68.3%–95.5% confidence contours for the *LMT* model with $z_t = 0.01$, using the CMB + BAO + Pantheon + RSD likelihoods.

III. COMPARISON OF DARK ENERGY MODELS

In order to truly resolve the H_0 tension, a dark energy model should not only provide a consistent measurement for M, but also maintain a quality of fit comparable (or even better) to ΛCDM with low-z data (BAO and SNIa), as discussed earlier. In this section, we consider some popular dark energy models that have been suggested as being capable of addressing the H_0 tension, following three different methods:

(1) Force all the models to be consistent with the Cepheid absolute magnitude measurement [170,174] at the 1σ level by imposing a flat prior $M \in [-19.28, -19.2]$ mag.

(2) Analyze all models including the local Cepheid-calibrated prior by SH0ES [170]:

$$M_c = -19.24 \pm 0.04 \text{ mag}. \tag{3.1}$$

(3) Include the SH0ES determination of H_0 [13], allowing at the same time the absolute magnitude M to vary freely (flat prior). This is illustrated in Appendix A as a complementary analysis.

The $H(z)$ deformation dark energy models that we consider in this work include the wCDM model, i.e. a model with a constant equation of state w, assuming a flat Universe and cold dark matter, that is described by a Hubble parameter of the form (neglecting radiation and neutrinos at late times)

$$H(z) = H_0\sqrt{\Omega_{\mathrm{m},0}(1+z)^3 + (1-\Omega_{\mathrm{m},0})(1+z)^{3(1+w)}}, \tag{3.2}$$

which for $w = -1$ reduces to the usual Hubble parameter for the ΛCDM model. Moreover, we consider the Chevallier-Polarski-Linder (CPL) parametrization, with a dark energy equation of state [193,194]

$$w(z) = w_0 + w_a\left(\frac{z}{1+z}\right), \tag{3.3}$$

where w_0 and w_a are free parameters. The corresponding Hubble parameter for the CPL model is the following:

$$H(z) = H_0\sqrt{\Omega_{\mathrm{m},0}(1+z)^3 + (1-\Omega_{\mathrm{m},0}) \times (1+z)^{3(1+w_0+w_a)}e^{-3\frac{w_a z}{1+z}}}. \tag{3.4}$$

Furthermore, we consider the phenomenologically emergent dark energy (PEDE) model which shows significant promise in resolving the H_0 problem. This model was introduced in Ref. [126] and has an equation of state of the form

$$w(z) = -\frac{1}{3\ln 10}(1 + \tanh[\log_{10}(1+z)]) - 1, \tag{3.5}$$

TABLE III. Constraints at 68.3% C.L. of the cosmological parameters for all the dark energy models explored in this work when a narrow flat prior $M \in [-19.28, -19.2]$ mag is assumed, forcing the agreement with Cepheid calibration [170,174] at the 1σ level. Note that this prior is artificial and the correct prior is the Gaussian one of Eq. (3.1) which is adopted in Table IV. For the transition models, M is fixed to -19.24 mag$(M_<)$. $\Delta\chi^2$ corresponds to the χ^2_{min} difference of each model with the ΛCDM case. All models provide a much better overall fit as compared to ΛCDM, and the *LwMT* and *LMT* models fair considerably better than the rest.

Parameters	ΛCDM	wCDM	CPL	*LwMT* ($z_t \geq 0.01$)	PEDE	*LMT* ($z_t = 0.01$)
$\Omega_{\mathrm{m},0}$	$0.2564^{+0.0018}_{-0.0019}$	$0.2571^{+0.0019}_{-0.0020}$	$0.2719^{+0.0041}_{-0.0044}$	0.3066 ± 0.0063	0.2582 ± 0.0020	0.3082 ± 0.0053
n_s	0.992 ± 0.003	0.972 ± 0.004	0.967 ± 0.004	0.968 ± 0.004	0.971 ± 0.003	0.968 ± 0.004
H_0	72.40 ± 0.16	$73.99^{+0.26}_{-0.27}$	72.38 ± 0.48	68.03 ± 0.55	$73.90^{+0.17}_{-0.19}$	67.89 ± 0.40
$\sigma_{8,0}$	$0.8045^{+0.0072}_{-0.0081}$	$0.8507^{+0.0084}_{-0.0083}$	$0.8511^{+0.0084}_{-0.0081}$	0.8088 ± 0.0063	0.8517 ± 0.0059	0.8084 ± 0.0059
S_8	0.7437 ± 0.0077	0.7876 ± 0.0084	0.8103 ± 0.0100	$0.8177^{+0.0101}_{-0.0103}$	0.7901 ± 0.0065	0.8194 ± 0.0100
M	~ -19.28	~ -19.28	~ -19.28	$-19.24(M_<)$	~ -19.28	$-19.24(M_<)$
ΔM	⋯	⋯	⋯	-0.170 ± 0.011	⋯	-0.172 ± 0.011
$M_> \equiv M_c + \Delta M$	⋯	⋯	⋯	-19.410 ± 0.011	⋯	-19.412 ± 0.011
Δw	⋯	⋯	⋯	Unconstrained	⋯	⋯
a_t	⋯	⋯	⋯	>0.987	⋯	⋯
w_0	⋯	$-1.162^{+0.021}_{-0.019}$	$-0.844^{+0.077}_{-0.089}$	⋯	⋯	⋯
w_a	⋯	⋯	$-1.27^{+0.38}_{-0.31}$	⋯	⋯	⋯
χ^2_{min}	3964	3889	3875	3834	3886	3835
$\Delta\chi^2_M$	⋯	−75	−89	−130	−78	−129

with a corresponding Hubble parameter of the form

$$H(z) = H_0\sqrt{(1-\Omega_{\mathrm{m},0}) \times [1-\tanh(\log_{10}(1+z))] + \Omega_{\mathrm{m},0}(1+z)^3}. \tag{3.6}$$

The main advantage of the aforementioned parametrization is that it has the same number of degrees of freedom as ΛCDM. Finally, we consider the transition models *LwMT* with $z_t > 0.01$ and *LMT* with $z_t = 0.01$ described in Sec. II, as well as the ΛCDM model itself, thus having a total of six different models.

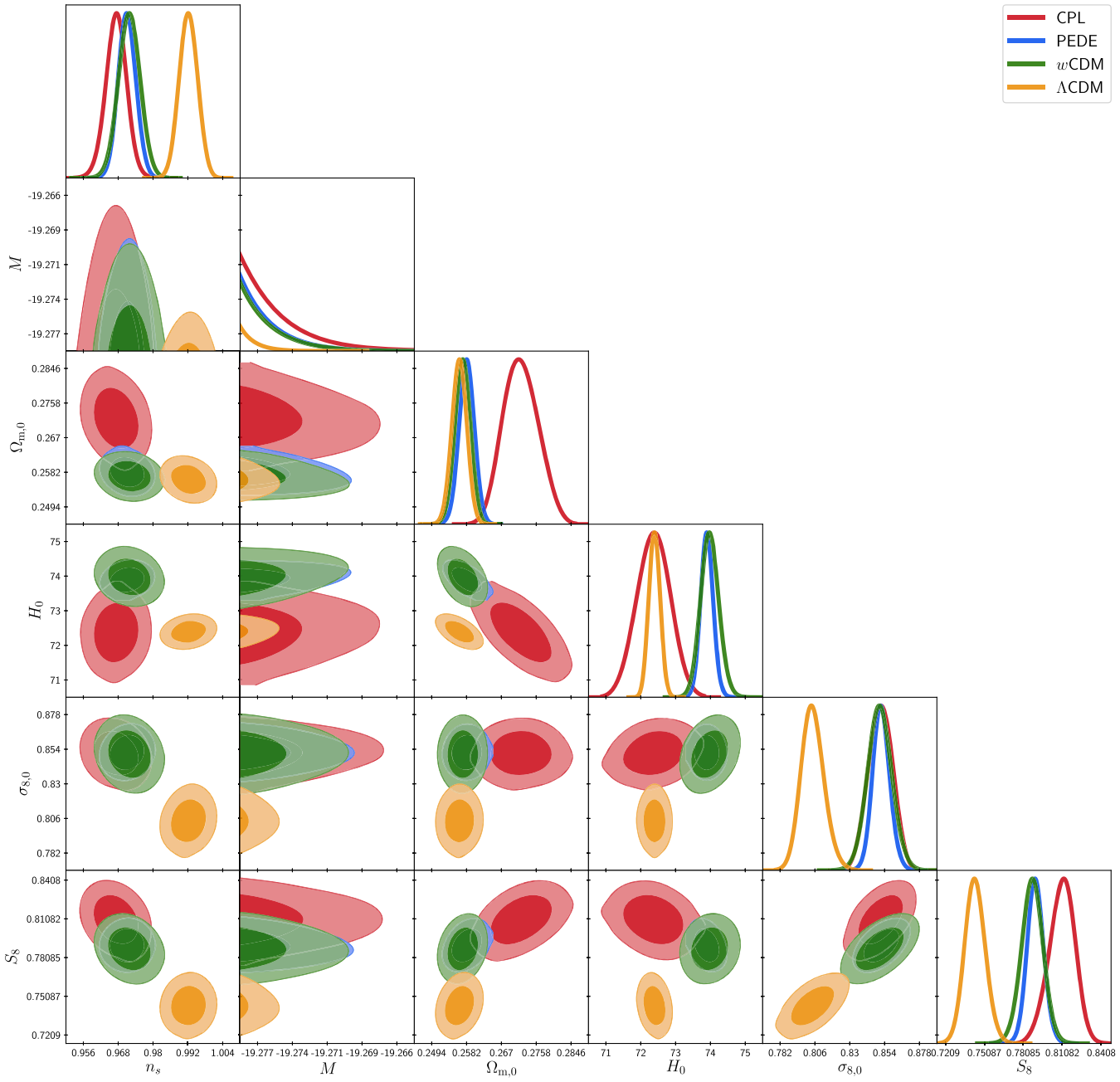

FIG. 4. The 68.3%–95.5% confidence contours for the common parameters of the ΛCDM, CPL, *w*CDM and PEDE dark energy models corresponding to the bounds illustrated in Table III. We used the CMB + BAO + Pantheon + RSD likelihoods, imposing the narrow flat prior $M \in [-19.28, -19.2]$ mag. The M prior severely constrains the best fit of M to the lowest possible value, displaying their tendency to provide a significantly lower value for M.

A. Dark energy models comparison using a narrow flat prior on $M \in [-19.28, -19.2]$ mag

We perform the MCMC analysis using the likelihoods described in Sec. II and imposing a narrow flat prior on the SNIa absolute magnitude $M \in [-19.28, -19.2]$ mag, that is, forcing all models to be consistent with the Cepheid measurement M_c. Rigorously, this prior is artificial as the correct prior is the Gaussian one of Eq. (3.1). However, the use of this narrow prior will be useful to understand the impact of the local calibration on the quality of fit of the various models.

For the transition models *LwMT* and *LMT*, we use Eq. (2.1) for the SNIa absolute magnitude and leave ΔM as a free variable. Thus, these are the only models that can, by construction, escape from the imposed M prior. The constraints on the cosmological parameters as well as the 68.3%–95.5% confidence contours of the corresponding parameters of the models are shown in Table III and Fig. 4, respectively. For the sake of clarity, contour plots for the *LMT* and *LwMT* models are displayed separately. In this case, the analysis with a narrow flat prior on M produces same constraints as those showed as Figs. 3 and 2 for the *LMT* and *LwMT* models, respectively. A wider flat prior would lead (as in the case of a Gaussian prior of Table IV that follows) the best fit value of M for most models to be very close to the CMB inferred value of $M = -19.4$ with an error bar which makes it inconsistent with the Cepheid inferred vale $M = -19.24$. In view of the degeneracy of M with H_0, this M tension is closely related with the H_0 tension. A similar (but milder) tension occurs also in the case of a Gaussian prior on M as indicated in Table IV.

All models, except the *LwMT* with $z_t \geq 0.01$ and *LMT* with $z_t = 0.01$, give an H_0 value that is consistent with the SH0ES determination of H_0 [13] and $M \sim -19.28$ mag, i.e. the lowest eligible value of the prior that we imposed, displaying their tendency to provide a significantly lower value for M. On the other hand, the transition models provide a H_0 value close (within the 1σ level) to the typical *Planck18*/ΛCDM value, providing at the same time $M \approx -19.4$ mag as expected.

Note that the ΛCDM model has a very bad fit to the data as compared to *w*CDM, CPL and PEDE. This is due to the fact that, having fixed M to the local M_c value, supernova data constrain the ΛCDM model's luminosity distance to values that are at odds with CMB and BAO. This clearly shows how the ΛCDM model cannot possibly solve the M crisis [170,171]. The more flexible *w*CDM, CPL and PEDE models fare much better but still much worse than the *LwMT* and *LMT* models which can fit all observables well.

All the models are forced to be consistent with the local Cepheid-calibrated value M_c at the 1σ level. As a result, in order to achieve consistency with M_c the values of the other parameters differ significantly from the relevant ΛCDM values. Also, the imposed significantly higher ($M > -19.28$) than the best fit inverse distance ladder value ($M = -19.4$) forces the MCMC process to restrict the rest of the parameters, thus explaining the extremely low uncertainties in order to achieve the best possible quality of fit to the data. We also stress that the peak structure of the CMB in the damping tail constrains very well the combination $\Omega_m h^2$. Therefore, once we force M-H_0 to be in agreement with SH0ES, we need a lower value of Ω_m different from ΛCDM to compensate for the higher H_0 value and keep the peak structure unaltered. Once we relax the M prior (Table IV) Ω_m can go back to the ΛCDM value.

TABLE IV. Constraints at 68.3% C.L. of the cosmological parameters for the dark energy models explored in this work when the prior $M = -19.24 \pm 0.04$ mag of Eq. (3.1) from SH0ES is adopted. $\Delta\chi^2$ corresponds to the $\chi^2_{\rm min}$ difference of each model with the ΛCDM case. Only transitions models provide a competitive fit to data as compared to ΛCDM.

Parameters	ΛCDM	*w*CDM	CPL	*LwMT* ($z_t \geq 0.01$)	PEDE	*LMT* ($z_t = 0.01$)
$\Omega_{\rm m,0}$	$0.3022^{+0.0051}_{-0.0052}$	0.2943 ± 0.0065	$0.2974^{+0.0067}_{-0.0068}$	$0.3073^{+0.0063}_{-0.0062}$	0.2789 ± 0.0049	0.3082 ± 0.0053
n_s	0.9704 ± 0.004	0.968 ± 0.004	0.967 ± 0.004	0.968 ± 0.004	0.963 ± 0.003	0.968 ± 0.004
H_0	68.36 ± 0.4	69.47 ± 0.72	69.25 ± 0.73	67.96 ± 0.55	71.85 ± 0.45	67.89 ± 0.40
$\sigma_{8,0}$	$0.8076^{+0.0058}_{-0.0062}$	$0.8215^{+0.0095}_{-0.0097}$	$0.8248^{+0.0096}_{-0.0097}$	$0.8084^{+0.0064}_{-0.0065}$	0.8531 ± 0.0059	0.8085 ± 0.0057
S_8	$0.8105^{+0.0097}_{-0.01}$	0.8135 ± 0.0098	$0.8210^{+0.0107}_{-0.0106}$	0.8181 ± 0.0100	0.8226 ± 0.0095	0.8194 ± 0.0099
M	-19.40 ± 0.01	-19.38 ± 0.02	-19.37 ± 0.02	-19.26 ± 0.04	-19.33 ± 0.01	-19.24 ± 0.04
ΔM	...	...	...	$-0.145^{+0.038}_{-0.035}$	...	-0.168 ± 0.039
$M_>$	...	...	...	-19.410 ± 0.011	...	-19.411 ± 0.011
Δw	...	...	...	Unconstrained	...	...
a_t	...	...	...	>0.986	...	...
w_0	...	-1.050 ± 0.027	-0.917 ± 0.078	...	...	...
w_a	...	...	$-0.53^{+0.33}_{-0.28}$	...	...	...
$\chi^2_{\rm min}$	3854	3851	3848	3833	3867	3835
$\Delta\chi^2$	...	−3	−6	−21	+13	−19

B. Dark energy models comparison using the local Cepheid prior on M

Here, we adopt the local Gaussian prior of Eq. (3.1). The constraints on cosmological parameters are given in Table IV, while the corresponding 68.3%–95.5% confidence contours are shown in Fig. 5. The transition $LwMT/LMT$ models fare significantly better than the other models, providing an absolute magnitude that is consistent with the Cepheid calibration of Eq. (3.1). The wCDM and CPL models achieve a slightly better fit to data as compared to ΛCDM, while the PEDE model has a significantly worse fit to data, in agreement with previous findings [127]. Note that constraints for the LMT and $LwMT$ models have been not included in Fig. 5 for the sake of clarity. Constraints for these model are instead showed in Fig. 8 of the Appendix B.

C. Model selection

To select the best model one cannot just look at the quality of fit but it is essential to include the information on

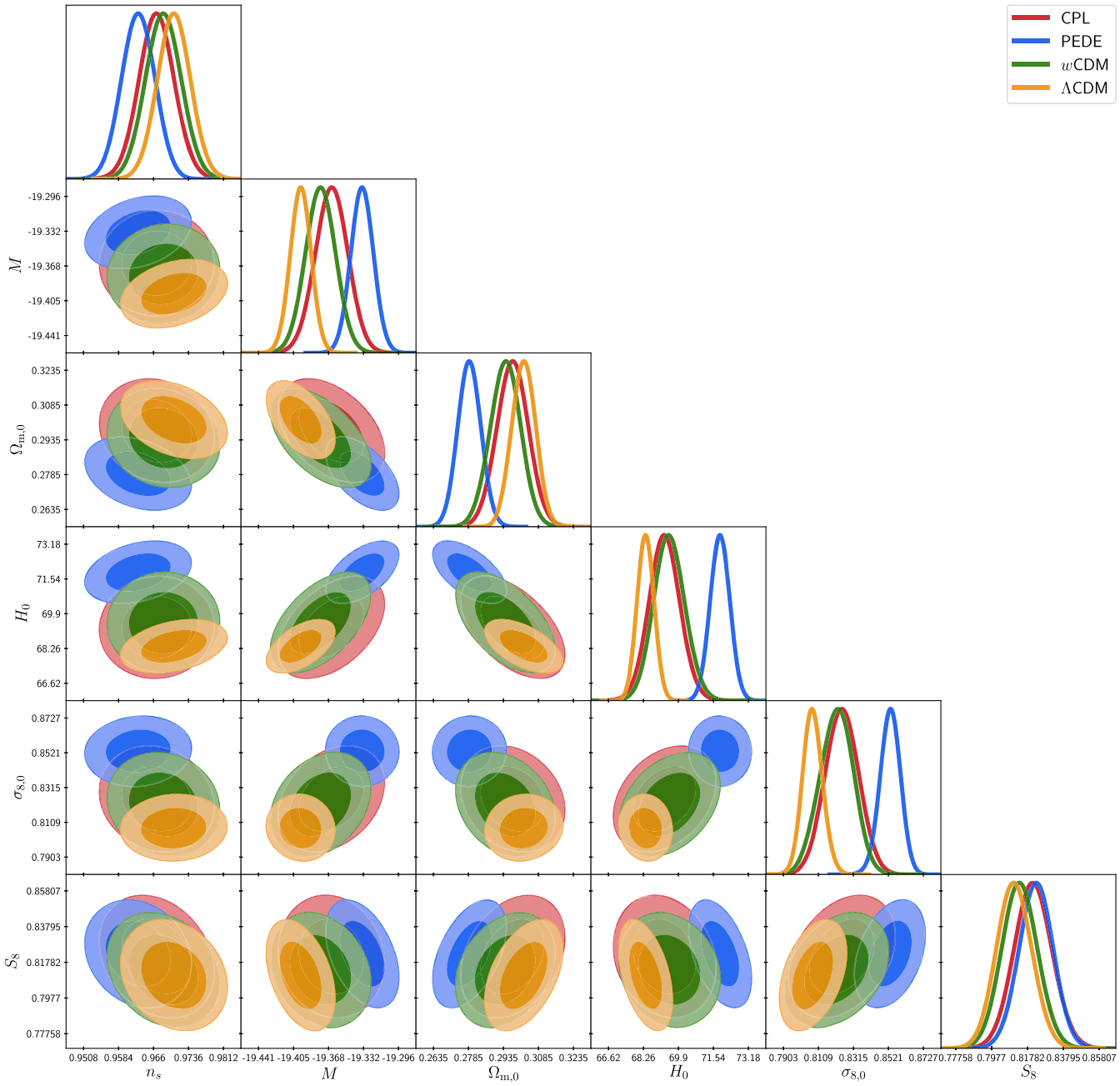

FIG. 5. The 68.3%–95.5% confidence contours for the common parameters of the CPL, wCDM and PEDE dark energy models with the prior $M = -19.24 \pm 0.04$ mag of Eq. (3.1) from SH0ES (corresponding bounds in Table IV).

the number of parameters and their priors. Here, we only consider the case of Sec. III B as it uses the actual Cepheid prior of Eq. (3.1) from SH0ES. We adopt two approaches. First, we consider the AIC [195,196], defined as

$$\mathrm{AIC} \equiv -2\ln\mathcal{L}_{\max} + 2N_{\mathrm{tot}} = \chi^2_{\min} + 2N_{\mathrm{tot}}, \quad (3.7)$$

where N_{tot} corresponds to the total number of free parameters of the considered model and $\mathcal{L}_{\max}$ corresponds to the maximum likelihood. This criterion penalizes a model for any extra parameters. Using Eq. (3.7) we calculate the AIC values for all the models of Table IV and construct the corresponding differences $\Delta\mathrm{AIC} \equiv AIC_{\mathrm{model}} - AIC_{\Lambda\mathrm{CDM}}$, see Table V. If $|\Delta\mathrm{AIC}| \leq 2$, then the compared models can be interpreted as consistent with each other, while if $|\Delta\mathrm{AIC}| \geq 4$, then it is an indication that the model with the larger AIC value is disfavored [196]. We can see that the $LwMT/LMT$ models are strongly favored over ΛCDM, and that the PEDE model is strongly disfavored.

We also use the MCEvidence package [197] in order to compute the Bayesian evidences (marginal likelihoods) of each model of Table IV using their respective MCMC chains. This algorithm obtains the posterior for the marginal likelihood, using the kth nearest-neighbor Mahalanobis distances [198] in the parameter space. In our analysis we have adopted the $k = 1$ case to minimize the effects of the inaccuracies associated with larger dimensions of the parameter space and smaller sample sizes. The strength of the evidence presented in favor or against a model in a comparison, can be found using the revised Jeffreys' scale [199]. Specifically, in a comparison between two models via the Bayes factor B (ratio of evidences), if $|\ln B| < 1$, then the models are comparable with none of them being favored. For $1 < |\ln B| < 2.5$ one model shows weak evidence in its favor: if $2.5 < |\ln B| < 5$, then the model in question has moderate evidence on its side. Lastly in the case of $|\ln B| > 5$ one model is strongly favored over the other. From Table V one can see that PEDE is strongly disfavored, wCDM and CPL weakly favored and disfavored, respectively, and that the $LwMT/LMT$ models are strongly favored over ΛCDM.

TABLE V. $\Delta\chi^2$ and corresponding ΔAIC and $\ln B$ values for all models of Table IV with respect to ΛCDM. Negative values of $\Delta\chi^2$ and ΔAIC and positive values of $\ln B$ signal that a model is favored with respect to ΛCDM.

Gaussian M prior case	$\Delta\chi^2$	ΔAIC	$\ln B$
ΛCDM	...	...	...
$LMT(z_t = 0.01)$	−19	−17	+9.1
$LwMT(z_t \geq 0.01)$	−21	−15	+6.2
wCDM	−3	−1	+2.2
CPL	−6	−2	−2.4
PEDE	+13	+13	−6.5

IV. DISCUSSION AND CONCLUSIONS

We have investigated the quality of fit to cosmological data of five models that attempt to solve the H_0 crisis. Besides the standard ΛCDM model, we considered three smooth $H(z)$ deformation models (wCDM, CPL, and PEDE) and two models that allow for a sudden transition of the SNIa absolute magnitude M at a recent cosmological redshift z_t. We performed model selection via the AIC and the Bayes factor. This is a more detailed and extended fit to the data that includes the full CMB angular power spectrum, instead of just the peak locations, discussed in the previous studies [84,155] that introduced the ultralate transition idea. We have also included additional cosmological models to compare the fit with the M transition models and implemented different priors and model selection criteria.

We found that the transition models are strongly favored with respect to the ΛCDM model. We also found that PEDE is strongly disfavored and that wCDM and CPL are weakly favored and disfavored, respectively. Specifically, only M-transition models are able to maintain consistency with the SNIa absolute magnitude M_c measured by Cepheid calibrators while at the same time maintaining a quality of fit to the cosmological data at $z > 0.01$ that is identical with that of ΛCDM.

The required transition with magnitude ΔM can be induced by a corresponding transition of the effective gravitational constant G_{eff} which determines the strength of the gravitational interactions [155]. The corresponding magnitude of the G_{eff} transition depends on the power value b of the expression that connects the evolving Newton's constant G_{eff} with the absolute luminosity L of a SNIa:

$$L \sim G^b_{\mathrm{eff}}. \quad (4.1)$$

In the case of the $LwMT$ and LMT transition models the transition in M implies a transition in $\mu \equiv G_{\mathrm{eff}}/G_{\mathrm{N}}$. In particular, for $z > z_t$, it is

$$\mu = 1 + \frac{\Delta G_{\mathrm{eff}}}{G_{\mathrm{N}}} \equiv 1 + \Delta\mu, \quad (4.2)$$

while for $z < z_t$ we have $\mu = 1$. Since, $\Delta\mu \ll 1$, we can assume without loss of generality that $\ln(1 + \Delta\mu) \simeq \Delta\mu$, so it is straightforward to show that Eq. (4.1) corresponds to

$$\Delta M = -\frac{5b}{2}\frac{\ln\mu}{\ln 10}. \quad (4.3)$$

Using the definition (4.2), for $z > z_t$, we have

$$\ln\mu \simeq \Delta M. \quad (4.4)$$

Therefore, substituting (4.4) in (4.3) and solving with respect to b, we derive

$$b = -\frac{2\ln 10}{5}\frac{\Delta M}{\Delta\mu}. \tag{4.5}$$

We can constrain b based on Eq. (4.5) and the fact that it obeys the general bounds $|b| \in [b_{\rm min}, +\infty)$ (the $+\infty$ corresponds to the ΛCDM /general relativity case where $\Delta\mu = 0$). Taking the absolute value of Eq. (4.5) and setting from Table II the 2-σ upper bound $|\Delta M|_{\rm min} = -0.172 + 2 \times 0.012 = -0.148$ mag and $|\Delta\mu|_{\rm min} = 0.05$ [200], a measurement obtained using up to date primitive element abundances, cosmic microwave background as well as nuclear and weak reaction rates, $b_{\rm min}$ assumes the following 2σ range

$$b_{\rm min,0.05} = (-\infty, -2.7] \cup [2.7, +\infty). \tag{4.6}$$

Similarly, if we consider the constraint from the Hubble diagram SNIa [201], a measurement derived using luminous red galaxies, as well as from Paleontology [202], a measurement obtained using the age of bacteria and algae, that indicate $|\Delta\mu|_{\rm min} = 0.1$, we derive

$$b_{\rm min,0.1} = (-\infty, -1.4] \cup [1.4, +\infty). \tag{4.7}$$

This range includes the simple expectation that emerges if we assume that the SNIa absolute luminosity is proportional to the Chandrasekhar mass $L \sim M_{\rm Ch} \sim G_{\rm eff}^{-3/2}$ which leads to $b = -3/2$.

If the M transition is due to a gravitational transition with a lower value of $G_{\rm eff}$ at $z > z_t$, then this class of models also has the potential to address the growth tension as discussed in previous studies [155]. It should also be stressed that such a gravitational transition would be consistent with Solar System tests of modified gravities without the need for screening since the value of $G_{\rm eff}$ is predicted to be constant at $z < z_t$, and therefore no modification of the planetary orbits is expected since the time these orbits have been monitored. However, at the time of the gravitational transition (about 100 Myrs ago) a disruption of the planetary orbits and comets is expected [203]. Such a prediction may be consistent with the observational fact that the rate of comets that hit the Earth and the Moon has increased by a factor of 2–3 during the past 100 Myrs [204–208].

As discussed in e.g. Refs. [209–211], SNIa progenitors are not necessarily Chandrasekhar-mass white dwarfs and a significant fraction can arise from sub-Chandrasekhar explosions. While this surely calls for a more detailed analysis of the dependence of the SNIa luminosity on $G_{\rm eff}$, one must note that the Chandrasekhar mass scale is a fundamental reference scale that plays an important role in all SNIa explosions. However, a nontrivial relation between progenitors and SNIa could again imply that the relation of Eq. (4.1) could feature a value of b different from $-3/2$ corresponding to the simplest case where $L \sim M_{\rm Chandra}$.

Therefore, interesting extensions of our analysis include the following:

(i) The search for traces or constraints of a gravitational transition in geological, Solar System and astrophysical data.
(ii) The construction of simple theoretical modified gravity models that can naturally induce the required transition of the effective Newton's $G_{\rm eff}$ at low redshifts ($z_t < 0.01$) perhaps avoiding fine tuning issues.
(iii) The possible identification of alternative non-gravitational physical mechanisms that could induce the transition of SNIa at low redshifts.
(iv) The search for systematic effects in the Cepheid data and parameters that could mimic such a transition and/or induce a higher value of M for SNIa than the one currently accepted.

In conclusion the M-transition class of models is an interesting new approach to the Hubble and possibly to the growth tension that deserves further investigation.

ACKNOWLEDGMENTS

The MCMC chains were produced in the Hydra cluster at the Instituto de Física Teórica (IFT) in Madrid and in the CHE cluster, managed and funded by COSMO/CBPF/MCTI, with financial support from FINEP and FAPERJ, and operating at the Javier Magnin Computing Center/CBPF, using MontePython/CLASS [187–189]. G. A.'s research was supported by the project "Dioni: Computing Infrastructure for Big-Data Processing and Analysis" (MIS Grant No. 5047222) cofunded by European Union (ERDF) and Greece through Operational Program "Competitiveness, Entrepreneurship and Innovation," NSRF 2014-2020. D. C. thanks CAPES for financial support. E. D. V. is supported by a Royal Society Dorothy Hodgkin Research Fellowship. L. K. is cofinanced by Greece and the European Union (European Social Fund-ESF) through the Operational Programme "Human Resources Development, Education and Lifelong Learning" in the context of the project "Strengthening Human Resources Research Potential via Doctorate Research—2nd Cycle" (Grant No. MIS-5000432), implemented by the State Scholarships Foundation (IKY). V. M. thanks CNPq (Brazil) and FAPES (Brazil) for partial financial support. This project has received funding from the European Union's Horizon 2020 research and innovation programme under the Marie Skłodowska-Curie Grant Agreement No. 888258. S. N. acknowledges support from the Research Project PGC2018-094773-B-C32, the Centro de Excelencia Severo Ochoa Program SEV-2016-0597 and the Ramón y Cajal program through Grant No. RYC-2014-15843.

Note.—The numerical analysis files for the reproduction of the figures can be found in the GitHub repository H0_Model_Comparison [212] under the MIT license.

APPENDIX A: ANALYSIS OF THE DARK ENERGY MODELS INCLUDING THE LOCAL H_0 MEASUREMENT

We repeat the analysis for the models in question including the latest SH0ES measurement, $H_0 = 73.2 \pm 1.3\ \mathrm{km\,s^{-1}\,Mpc^{-1}}$ [13], instead of the local prior on M of Eq. (3.1) that was adopted in Sec. III B. This is done in order to show that, despite the strong constraining nature of the SH0ES measurement, the obtained absolute magnitude M for smooth $H(z)$ deformation models are inconsistent with the measured Cepheid absolute magnitude $M_c = -19.24 \pm 0.04$ mag of Eq. (3.1). It is worth stressing that it is preferable to adopt the local prior on M for the following reasons [170]: (i) one avoids double counting low-z supernova, (ii) the statistical information on M is included in the analysis and (iii) one avoids adopting a low-z cosmography, with possibly wrong parameters, in the analysis.

Repeating the MCMC analysis and using the same likelihoods described in Sec. II, we obtain the constraints on cosmological parameters for all the models as shown in Table VI. The corresponding 68.3%–95.5% confidence contours of the common parameters of the models are illustrated in Fig. 6. Constraints for the *LMT* and *LwMT* models have been not included in Fig. 6, instead we show those constraints in Fig. 9.

Clearly, all of the considered models (except the models with transitions) tend to prefer a significantly lower value for M (which is considered to be constant) compared to M_c. This is also evident in Fig. 7, where the best fit absolute magnitude M of the binned Pantheon data is shown. In particular, in the case where no prior on M is imposed, two of the considered models, i.e. wCDM and CPL, produce a H_0 best fit value that is inconsistent with the SH0ES measurement [13] at more than 2.4σ. Regarding the *LwMT* with $(z_t \geq 0.01)$, even with the SH0ES measurement, the best fit value of a_t parameter remains unaffected, continuing to favor a transition at very low redshifts. Conclusively, even though the majority of dark energy models discussed in this work (except PEDE and *LMT*) display a better quality of fit to the data than that of ΛCDM (cyan row of Table VI), they fail to give an M value consistent with the M_c measurement (except the *LwMT* and *LMT* models) despite the fact that some of them (such as PEDE) provide a H_0 measurement, that is consistent with the SH0ES measurement at the 1σ level.

TABLE VI. Constraints at 68% C.L. of the basic parameters for all the considered dark energy models, including the SH0ES measurement $H_0 = 73.2 \pm 1.3\ \mathrm{km\,s^{-1}\,Mpc^{-1}}$ [13]. Clearly all the considered dark energy models except the *LwMT* model with $z_t \geq 0.01$ and *LMT* with $z_t = 0.01$ give a SNIa absolute magnitude M that is inconsistent with the local calibration $M_c = -19.24 \pm 0.04$ mag of Eq. (3.1). However, this statistical inconsistency is not included in the χ^2 that is used to interpret the results, see discussion in [170].

Parameters	ΛCDM	wCDM	CPL	*LwMT* $(z_t \geq 0.01)$	PEDE	*LMT* $(z_t = 0.01)$
$\Omega_{\mathrm{m},0}$	$0.3022^{+0.0050}_{-0.0052}$	$0.2967^{+0.0067}_{-0.0064}$	$0.2951^{+0.0063}_{-0.0067}$	$0.2989^{+0.0055}_{-0.0060}$	0.281 ± 0.005	$0.3021^{+0.0053}_{-0.0052}$
n_s	0.9705 ± 0.0037	0.9684 ± 0.004	0.9668 ± 0.0040	0.9706 ± 0.0037	$0.9621^{+0.0036}_{-0.0034}$	0.9705 ± 0.0038
H_0	68.36 ± 0.4	$69.17^{+0.65}_{-0.76}$	69.50 ± 0.71	68.71 ± 0.5	$71.69^{+0.45}_{-0.46}$	$68.36^{+0.40}_{-0.41}$
$\sigma_{8,0}$	$0.8075^{+0.0058}_{-0.0064}$	$0.8183^{+0.0089}_{-0.01}$	0.8258 ± 0.0099	0.8098 ± 0.0064	$0.8531^{0.0064}_{-0.0058}$	$0.8086^{+0.0058}_{-0.0064}$
M	-19.40 ± 0.01	-19.38 ± 0.02	$-19.37^{+0.017}_{-0.018}$	-19.24	-19.34 ± 0.01	-19.24
ΔM	⋯	⋯	⋯	-0.1652 ± 0.011	⋯	-0.159 ± 0.011
$M_> \equiv M_c + \Delta M$	⋯	⋯	⋯	-19.405 ± 0.011	⋯	-19.40 ± 0.011
Δw	⋯	⋯	⋯	> -0.7	⋯	⋯
a_t	⋯	⋯	⋯	>0.98	⋯	⋯
w_0	⋯	$-1.038^{+0.031}_{-0.018}$	$-0.9576^{+0.075}_{-0.078}$	⋯	⋯	⋯
w_a	⋯	⋯	$-0.38^{+0.32}_{-0.27}$	⋯	⋯	⋯
χ^2	3849	3846	3845	3846	3862	3850
$\Delta\chi^2$	⋯	−3	−4	−3	+13	+1

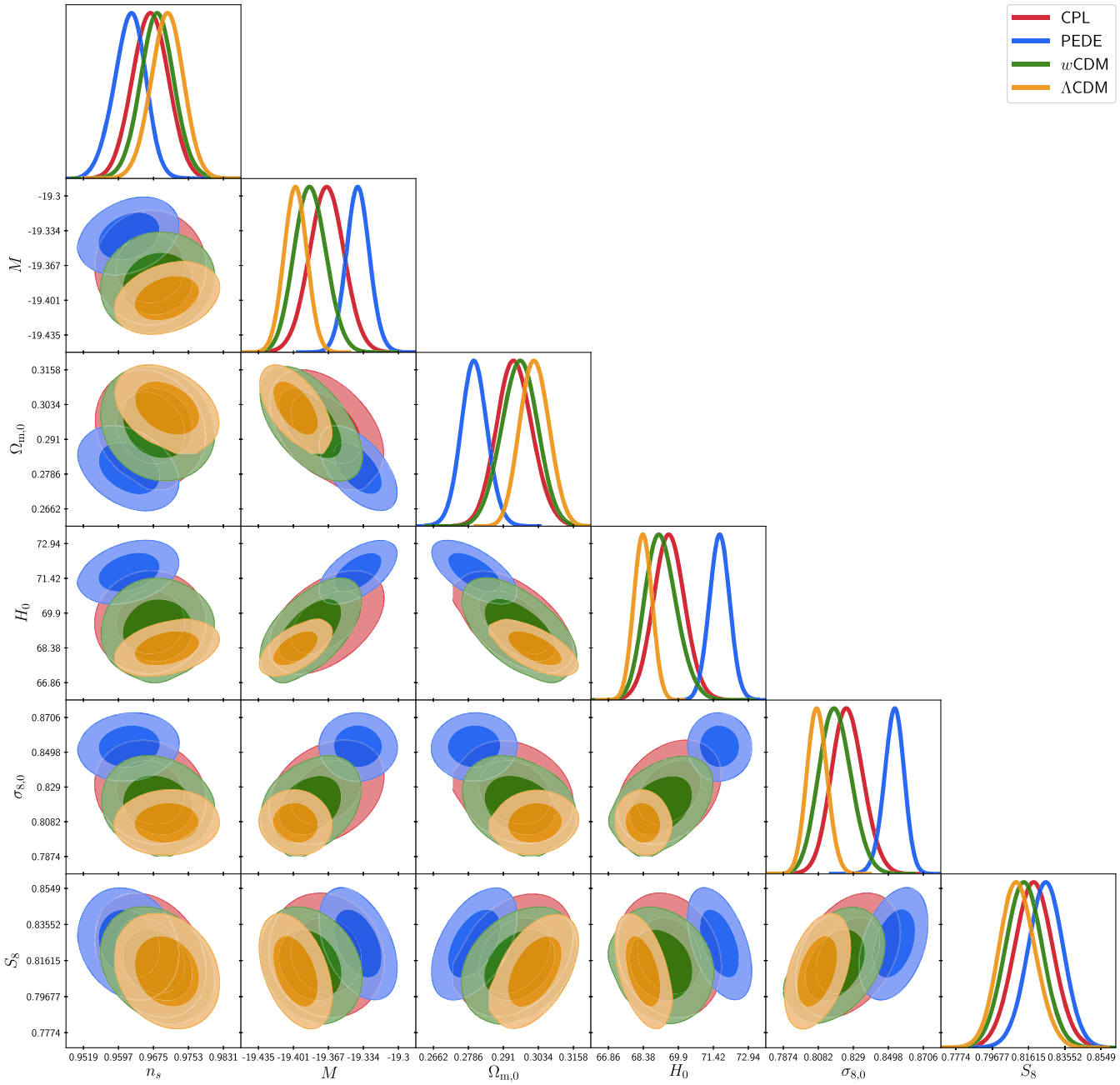

FIG. 6. The 68.3%–95.5% confidence contours for the common parameters of the ΛCDM, CPL, wCDM, and PEDE dark energy models corresponding to the constraints given in Table VI. We used the CMB + BAO + Pantheon + RSD likelihoods, including the SH0ES measurement $H_0 = 73.2 \pm 1.3$ km s^{-1} Mpc^{-1} [13]. The M value of the models is inconsistent with the local calibration of Eq. (3.1) ($M_c = -19.24 \pm 0.04$ mag).

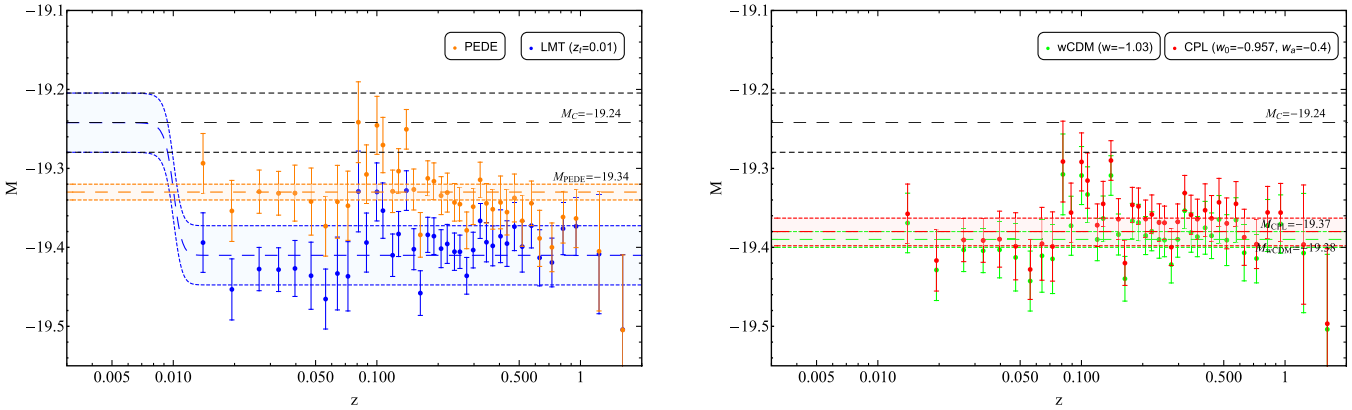

FIG. 7. The best fit absolute magnitude M of the binned Pantheon data as a function of the redshift z. In the left panel we show the corresponding best fit data for the LMT model with $z_t = 0.01$ (blue points) and PEDE models (orange points). In the right panel we show the corresponding best fit data for the wCDM model with $w = -1.03$ (green points) and CPL models (red points). Clearly, all the models provide a value that is inconsistent with the measured Cepheid absolute magnitude M_c (straight dashed lines), unless a model with a transition on M (such as LMT) is considered.

APPENDIX B: CONTOURS PLOTS FOR THE *LMT* and *LwMT* MODELS

Here, we show contours plots relative to analyses with the models *LMT* and *LwMT*. Figure 8 shows the 68.3%–95.5% confidence contours of cosmological parameters of models *LMT* and *LwMT* for the analysis with the Gaussian prior on M. On the other hand, Fig. 9 shows the 68.3%–95.5% confidence contours of cosmological parameters of models *LMT* and *LwMT* for the analysis that includes a Gaussian prior on H_0.

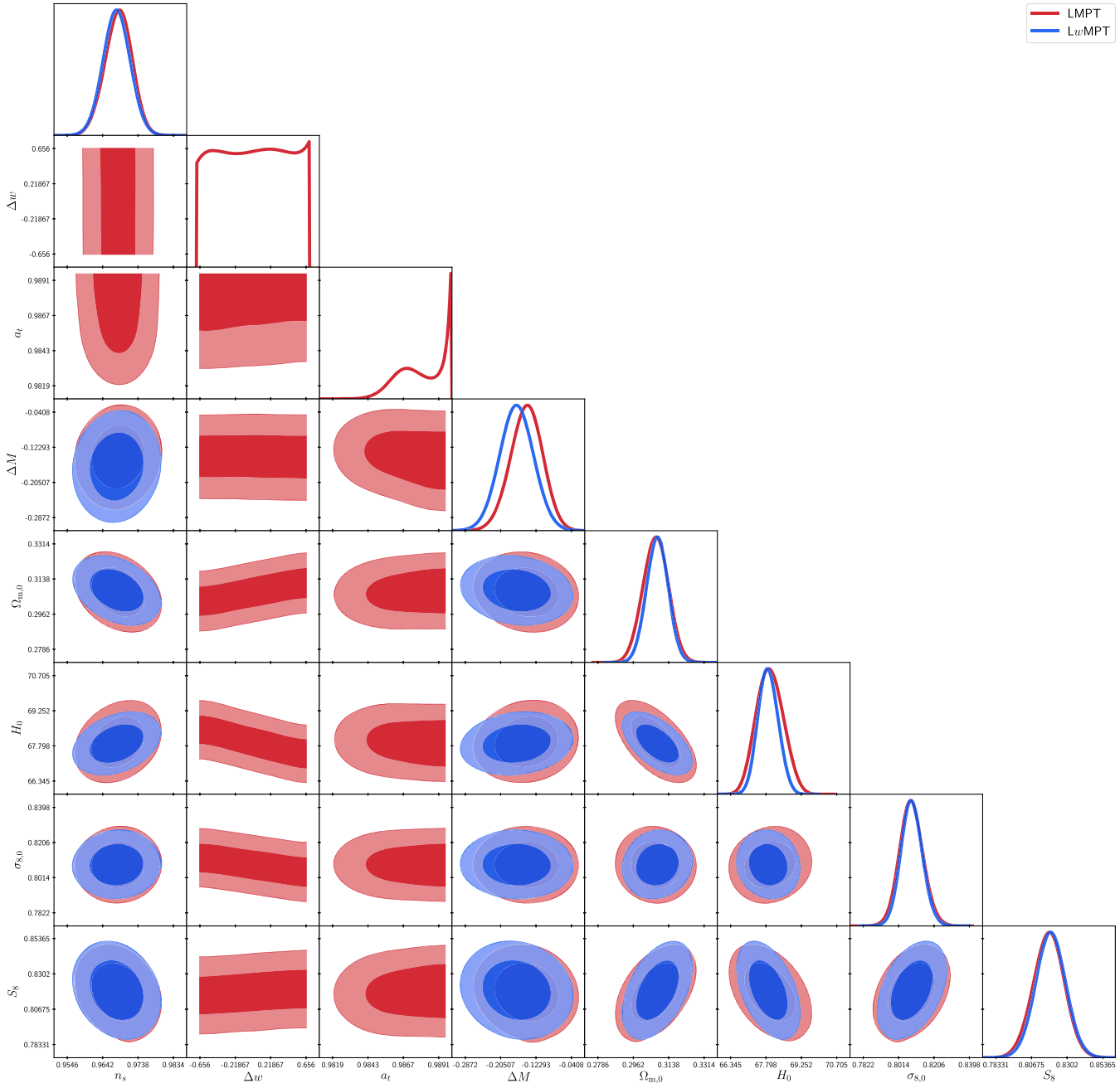

FIG. 8. The 68.3%–95.5% confidence contours of the *LMT*, and *LwMT* dark energy models with the prior $M = -19.24 \pm 0.04$ mag of Eq. (3.1) from SH0ES (corresponding bounds in Table IV).

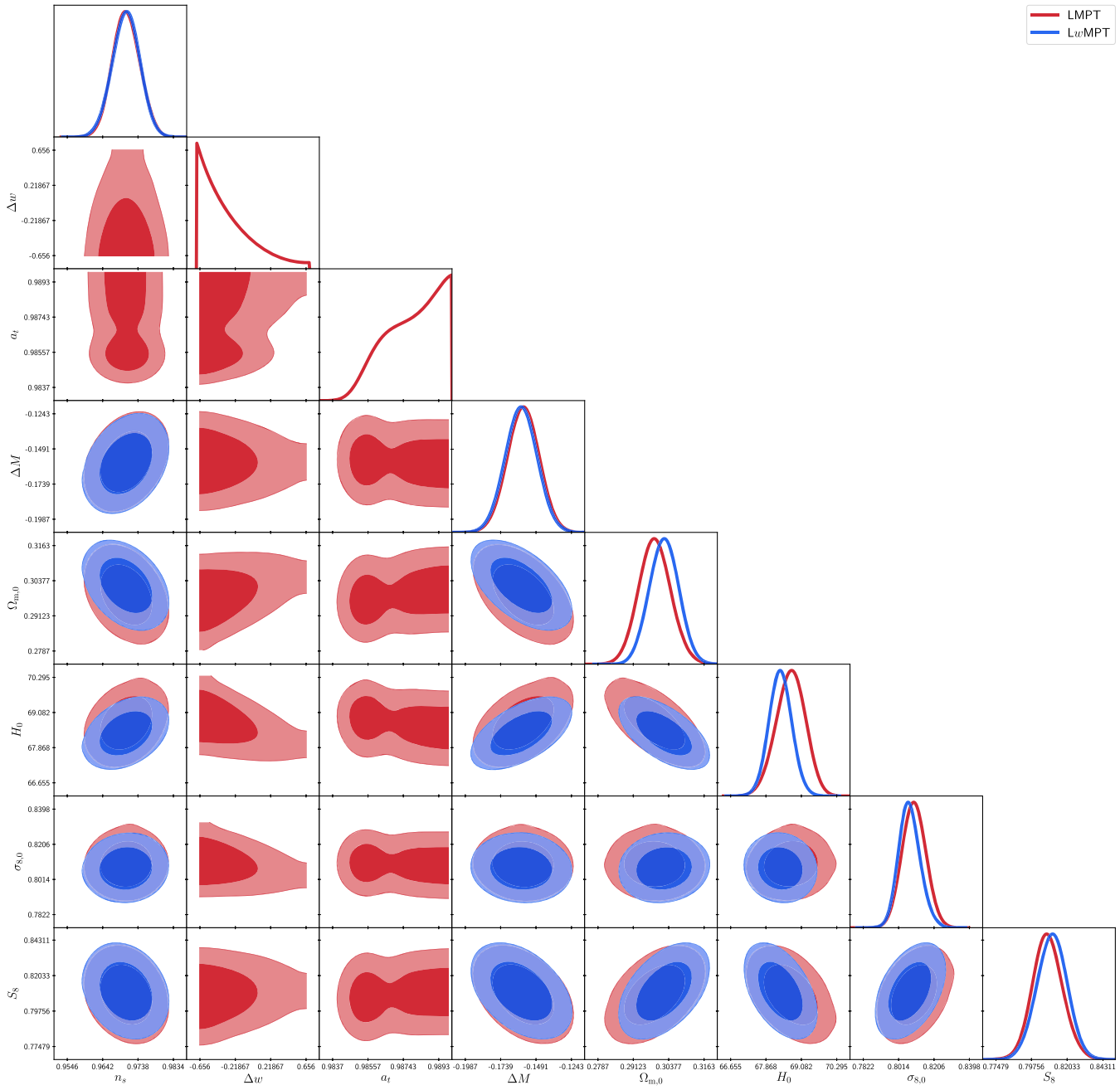

FIG. 9. The 68.3%–95.5% confidence contours for the common parameters of the *LMT* and *LwMT* dark energy models corresponding to the constraints given in Table VI. We used the CMB + BAO + Pantheon + RSD likelihoods, including the SH0ES measurement $H_0 = 73.2 \pm 1.3$ km s^{-1} Mpc^{-1} [13].

[1] Eleonora Di Valentino *et al.*, Snowmass2021—Letter of interest cosmology intertwined I: Perspectives for the next decade, Astropart. Phys. **131**, 102606 (2021).
[2] Eleonora Di Valentino *et al.*, Snowmass2021—Letter of interest cosmology intertwined II: The Hubble constant tension, Astropart. Phys. **131**, 102605 (2021).
[3] Eleonora Di Valentino *et al.*, Cosmology intertwined III: $f\sigma_8$ and S_8, Astropart. Phys. **131**, 102604 (2021).
[4] Eleonora Di Valentino *et al.*, Snowmass2021—Letter of interest cosmology intertwined IV: The age of the universe and its curvature, Astropart. Phys. **131**, 102607 (2021).

[5] Leandros Perivolaropoulos and Foteini Skara, Challenges for ΛCDM: An update, arXiv:2105.05208.

[6] Emmanuel N. Saridakis *et al.* (CANTATA Collaboration), Modified gravity and cosmology: An update by the CANTATA network, arXiv:2105.12582.

[7] L. Verde, T. Treu, and A. G. Riess, Tensions between the early and the late universe, Nat. Astron. **3**, 891 (2019).

[8] Adam G. Riess, The expansion of the universe is faster than expected, Nat. Rev. Phys. **2**, 10 (2020).

[9] Eleonora Di Valentino, A combined analysis of the H_0 late time direct measurements and the impact on the Dark Energy sector, Mon. Not. R. Astron. Soc. **502**, 2065 (2021).

[10] Eleonora Di Valentino, Olga Mena, Supriya Pan, Luca Visinelli, Weiqiang Yang, Alessandro Melchiorri, David F. Mota, Adam G. Riess, and Joseph Silk, In the realm of the Hubble tension—a review of solutions, Classical Quantum Gravity **38**, 153001 (2021).

[11] Paul Shah, Pablo Lemos, and Ofer Lahav, A buyer's guide to the Hubble Constant, Astron. Astrophys. Rev. **29**, 9 (2021).

[12] N. Aghanim *et al.* (Planck Collaboration), Planck 2018 results. VI. Cosmological parameters, Astron. Astrophys. **641**, A6 (2020).

[13] Adam G. Riess, Stefano Casertano, Wenlong Yuan, J. Bradley Bowers, Lucas Macri, Joel C. Zinn, and Dan Scolnic, Cosmic distances calibrated to 1% precision with gaia EDR3 parallaxes and Hubble space telescope photometry of 75 Milky Way cepheids confirm tension with ΛCDM, Astrophys. J. Lett. **908**, L6 (2021).

[14] Simone Aiola *et al.* (ACT Collaboration), The atacama cosmology telescope: DR4 maps and cosmological parameters, J. Cosmol. Astropart. Phys. 12 (2020) 047.

[15] D. Dutcher *et al.* (SPT-3G Collaboration), Measurements of the E-mode polarization and temperature-E-mode correlation of the CMB from SPT-3G 2018 data, Phys. Rev. D **104**, 022003 (2021).

[16] Shadab Alam *et al.* (eBOSS Collaboration), Completed SDSS-IV extended Baryon Oscillation Spectroscopic Survey: Cosmological implications from two decades of spectroscopic surveys at the Apache Point Observatory, Phys. Rev. D **103**, 083533 (2021).

[17] John Soltis, Stefano Casertano, and Adam G. Riess, The parallax of ω centauri measured from gaia EDR3 and a direct, geometric calibration of the tip of the red giant branch and the Hubble constant, Astrophys. J. Lett. **908**, L5 (2021).

[18] D. W. Pesce *et al.*, The megamaser cosmology project. XIII. Combined Hubble constant constraints, Astrophys. J. Lett. **891**, L1 (2020).

[19] Ehsan Kourkchi, R. Brent Tully, Gagandeep S. Anand, Helene M. Courtois, Alexandra Dupuy, James D. Neill, Luca Rizzi, and Mark Seibert, Cosmicflows-4: The calibration of optical and infrared Tully–Fisher relations, Astrophys. J. **896**, 3 (2020).

[20] James Schombert, Stacy McGaugh, and Federico Lelli, Using the baryonic Tully–Fisher relation to measure H o, Astron. J. **160**, 71 (2020).

[21] John P. Blakeslee, Joseph B. Jensen, Chung-Pei Ma, Peter A. Milne, and Jenny E. Greene, The Hubble constant from infrared surface brightness fluctuation distances, Astrophys. J. **911**, 65 (2021).

[22] Wendy L. Freedman, Measurements of the Hubble constant: Tensions in perspective, Astrophys. J. **919**, 16 (2021).

[23] Gagandeep S. Anand, R. Brent Tully, Luca Rizzi, Adam G. Riess, and Wenlong Yuan, Comparing tip of the red giant branch distance scales: An independent reduction of the Carnegie-Chicago Hubble program and the value of the Hubble constant, arXiv:2108.00007.

[24] S. Birrer *et al.*, TDCOSMO—IV. Hierarchical time-delay cosmography—joint inference of the Hubble constant and galaxy density profiles, Astron. Astrophys. **643**, A165 (2020).

[25] H. Hildebrandt *et al.*, KiDS-450: Cosmological parameter constraints from tomographic weak gravitational lensing, Mon. Not. R. Astron. Soc. **465**, 1454 (2017).

[26] Savvas Nesseris, George Pantazis, and Leandros Perivolaropoulos, Tension and constraints on modified gravity parametrizations of $G_{\rm eff}(z)$ from growth rate and Planck data, Phys. Rev. D **96**, 023542 (2017).

[27] Edward Macaulay, Ingunn Kathrine Wehus, and Hans Kristian Eriksen, Lower Growth Rate from Recent Redshift Space Distortion Measurements than Expected from Planck, Phys. Rev. Lett. **111**, 161301 (2013).

[28] Lavrentios Kazantzidis and Leandros Perivolaropoulos, Evolution of the $f\sigma_8$ tension with the Planck15/ΛCDM determination and implications for modified gravity theories, Phys. Rev. D **97**, 103503 (2018).

[29] F. Skara and L. Perivolaropoulos, Tension of the E_G statistic and redshift space distortion data with the Planck—ΛCDM model and implications for weakening gravity, Phys. Rev. D **101**, 063521 (2020).

[30] Lavrentios Kazantzidis and Leandros Perivolaropoulos, Is gravity getting weaker at low z? Observational evidence and theoretical implications, arXiv:1907.03176.

[31] Leandros Perivolaropoulos and Lavrentios Kazantzidis, Hints of modified gravity in cosmos and in the lab?, Int. J. Mod. Phys. D **28**, 1942001 (2019).

[32] Tanvi Karwal and Marc Kamionkowski, Dark energy at early times, the Hubble parameter, and the string axiverse, Phys. Rev. D **94**, 103523 (2016).

[33] Vivian Poulin, Tristan L. Smith, Tanvi Karwal, and Marc Kamionkowski, Early Dark Energy Can Resolve The Hubble Tension, Phys. Rev. Lett. **122**, 221301 (2019).

[34] Jeremy Sakstein and Mark Trodden, Early Dark Energy from Massive Neutrinos as a Natural Resolution of the Hubble Tension, Phys. Rev. Lett. **124**, 161301 (2020).

[35] Florian Niedermann and Martin S. Sloth, New early dark energy, Phys. Rev. D **103**, L041303 (2021).

[36] J. Colin Hill, Evan McDonough, Michael W. Toomey, and Stephon Alexander, Early dark energy does not restore cosmological concordance, Phys. Rev. D **102**, 043507 (2020).

[37] Riccardo Murgia, Guillermo F. Abellán, and Vivian Poulin, Early dark energy resolution to the Hubble tension in light of weak lensing surveys and lensing anomalies, Phys. Rev. D **103**, 063502 (2021).

[38] Guido D'Amico, Leonardo Senatore, Pierre Zhang, and Henry Zheng, The Hubble tension in light of the full-shape

analysis of large-scale structure data, J. Cosmol. Astropart. Phys. 05 (2021) 072.
[39] Antareep Gogoi, Ravi Kumar Sharma, Prolay Chanda, and Subinoy Das, Early mass-varying neutrino dark energy: Nugget formation and Hubble anomaly, Astrophys. J. **915**, 132 (2021).
[40] Anton Chudaykin, Dmitry Gorbunov, and Nikita Nedelko, Exploring an early dark energy solution to the Hubble tension with Planck and SPTPol data, Phys. Rev. D **103**, 043529 (2021).
[41] Anton Chudaykin, Dmitry Gorbunov, and Nikita Nedelko, Combined analysis of Planck and SPTPol data favors the early dark energy models, J. Cosmol. Astropart. Phys. 08 (2020) 013.
[42] Prateek Agrawal, Francis-Yan Cyr-Racine, David Pinner, and Lisa Randall, Rock 'n' roll solutions to the Hubble tension, arXiv:1904.01016.
[43] Florian Niedermann and Martin S. Sloth, Resolving the Hubble tension with new early dark energy, Phys. Rev. D **102**, 063527 (2020).
[44] Gen Ye and Yun-Song Piao, Is the Hubble tension a hint of AdS phase around recombination?, Phys. Rev. D **101**, 083507 (2020).
[45] Meng-Xiang Lin, Giampaolo Benevento, Wayne Hu, and Marco Raveri, Acoustic dark energy: Potential conversion of the Hubble tension, Phys. Rev. D **100**, 063542 (2019).
[46] Matteo Braglia, William T. Emond, Fabio Finelli, A. Emir Gumrukcuoglu, and Kazuya Koyama, Unified framework for Early Dark Energy from α-attractors, Phys. Rev. D **102**, 083513 (2020).
[47] J. Colin Hill *et al.*, The atacama cosmology telescope: Constraints on pre-recombination early dark energy, arXiv:2109.04451.
[48] Chia-Feng Chang, Imprint of early dark energy in stochastic gravitational wave background, Phys. Rev. D **105**, 023508 (2022).
[49] Gen Ye, Jun Zhang, and Yun-Song Piao, Resolving both H_0 and S_8 tensions with AdS early dark energy and ultralight axion, arXiv:2107.13391.
[50] Adrià Gómez-Valent, Ziyang Zheng, Luca Amendola, Valeria Pettorino, and Christof Wetterich, Early dark energy in the pre- and post-recombination epochs, Phys. Rev. D **104**, 083536 (2021).
[51] Jun-Qian Jiang and Yun-Song Piao, Testing AdS early dark energy with Planck, SPTpol and LSS data, Phys. Rev. D **104**, 103524 (2021).
[52] Tanvi Karwal, Marco Raveri, Bhuvnesh Jain, Justin Khoury, and Mark Trodden, Chameleon early dark energy and the Hubble tension, arXiv:2106.13290.
[53] Vivian Poulin, Tristan L. Smith, and Alexa Bartlett, Dark energy at early times and ACT: A larger Hubble constant without late-time priors, Phys. Rev. D **104**, 123550 (2021).
[54] Sunny Vagnozzi, New physics in light of the H_0 tension: An alternative view, Phys. Rev. D **102**, 023518 (2020).
[55] Osamu Seto and Yo Toda, Comparing early dark energy and extra radiation solutions to the Hubble tension with BBN, Phys. Rev. D **103**, 123501 (2021).
[56] S. Carneiro, P. C. de Holanda, C. Pigozzo, and F. Sobreira, Is the H_0 tension suggesting a fourth neutrino generation?, Phys. Rev. D **100**, 023505 (2019).
[57] Graciela B. Gelmini, Alexander Kusenko, and Volodymyr Takhistov, Possible hints of sterile neutrinos in recent measurements of the Hubble parameter, J. Cosmol. Astropart. Phys. 06 (2021) 002.
[58] Graciela B. Gelmini, Masahiro Kawasaki, Alexander Kusenko, Kai Murai, and Volodymyr Takhistov, Big bang nucleosynthesis constraints on sterile neutrino and lepton asymmetry of the Universe, J. Cosmol. Astropart. Phys. 09 (2020) 051.
[59] Francesco D'Eramo, Ricardo Z. Ferreira, Alessio Notari, and José Luis Bernal, Hot axions and the H_0 tension, J. Cosmol. Astropart. Phys. 11 (**2018**) 014.
[60] Kanhaiya L. Pandey, Tanvi Karwal, and Subinoy Das, Alleviating the H_0 and σ_8 anomalies with a decaying dark matter model, J. Cosmol. Astropart. Phys. 07 (2020) 026.
[61] Linfeng Xiao, Le Zhang, Rui An, Chang Feng, and Bin Wang, Fractional dark matter decay: Cosmological imprints and observational constraints, J. Cosmol. Astropart. Phys. 01 (2020) 045.
[62] Andreas Nygaard, Thomas Tram, and Steen Hannestad, Updated constraints on decaying cold dark matter, J. Cosmol. Astropart. Phys. 05 (**2021**) 017.
[63] Nikita Blinov, Celeste Keith, and Dan Hooper, Warm decaying dark matter and the Hubble tension, J. Cosmol. Astropart. Phys. 06 (2020) 005.
[64] Tobias Binder, Michael Gustafsson, Ayuki Kamada, Stefan Marinus Rodrigues Sandner, and Max Wiesner, Reannihilation of self-interacting dark matter, Phys. Rev. D **97**, 123004 (2018).
[65] Gongjun Choi, Motoo Suzuki, and Tsutomu T. Yanagida, Quintessence axion dark energy and a solution to the Hubble tension, Phys. Lett. B **805**, 135408 (2020).
[66] Eleonora Di Valentino, Céline Bøehm, Eric Hivon, and François R. Bouchet, Reducing the H_0 and σ_8 tensions with Dark Matter-neutrino interactions, Phys. Rev. D **97**, 043513 (2018).
[67] Miguel Escudero and Samuel J. Witte, A CMB search for the neutrino mass mechanism and its relation to the Hubble tension, Eur. Phys. J. C **80**, 294 (2020).
[68] Fernando Arias-Aragon, Enrique Fernandez-Martinez, Manuel Gonzalez-Lopez, and Luca Merlo, Neutrino masses and Hubble tension via a majoron in MFV, Eur. Phys. J. C **81**, 28 (2021).
[69] Nikita Blinov and Gustavo Marques-Tavares, Interacting radiation after Planck and its implications for the Hubble Tension, J. Cosmol. Astropart. Phys. 09 (2020) 029.
[70] V. V. Flambaum and I. B. Samsonov, Ultralight dark photon as a model for early universe dark matter, Phys. Rev. D **100**, 063541 (2019).
[71] Luis A. Anchordoqui, Eleonora Di Valentino, Supriya Pan, and Weiqiang Yang, Dissecting the H0 and S8 tensions with Planck + BAO + supernova type Ia in multi-parameter cosmologies, J. High Energy Astrophys. **32**, 28 (2021).
[72] Anirban Das, Self-interacting neutrinos as a solution to the hubble tension?, in *EPS Conference on High Energy Physics 2021* (2021), arXiv:2109.03263.
[73] Enrique Fernandez-Martinez, Mathias Pierre, E. Pinsard, and Salvador Rosauro-Alcaraz, Inverse Seesaw, dark matter and the Hubble tension, Eur. Phys. J. C **81**, 954 (2021).

[74] Lu Feng, Rui-Yun Guo, Jing-Fei Zhang, and Xin Zhang, Cosmological search for sterile neutrinos after Planck 2018, Phys. Lett. B **827**, 136940 (2022).

[75] Subhajit Ghosh, Soubhik Kumar, and Yuhsin Tsai, Free-streaming and coupled dark radiation isocurvature perturbations: constraints and application to the Hubble tension, arXiv:2107.09076.

[76] Dhiraj Kumar Hazra, Arman Shafieloo, and Tarun Souradeep, Parameter discordance in Planck CMB and low-redshift measurements: Projection in the primordial power spectrum, J. Cosmol. Astropart. Phys. 04 (2019) 036.

[77] Ryan E. Keeley, Arman Shafieloo, Dhiraj Kumar Hazra, and Tarun Souradeep, Inflation wars: A new hope, J. Cosmol. Astropart. Phys. 09 (**2020**) 055.

[78] Savvas Nesseris, Domenico Sapone, and Spyros Sypsas, Evaporating primordial black holes as varying dark energy, Phys. Dark Universe **27**, 100413 (2020).

[79] Nikki Arendse *et al.*, Cosmic dissonance: Are new physics or systematics behind a short sound horizon?, Astron. Astrophys. **639**, A57 (2020).

[80] Weikang Lin, Xingang Chen, and Katherine J. Mack, Early-universe-physics insensitive and uncalibrated cosmic standards: Constraints on Ω_m and implications for the Hubble tension, Astrophys. J. **920**, 159 (2021).

[81] Nils Schöneberg, Guillermo Franco Abellán, Andrea Pérez Sánchez, Samuel J. Witte, Vivian Poulin, and Julien Lesgourgues, The H_0 olympics: A fair ranking of proposed models, arXiv:2107.10291.

[82] Karsten Jedamzik, Levon Pogosian, and Gong-Bo Zhao, Why reducing the cosmic sound horizon can not fully resolve the Hubble tension, Commun. Phys. **4**, 123 (2021).

[83] Tristan L. Smith, Vivian Poulin, José Luis Bernal, Kimberly K. Boddy, Marc Kamionkowski, and Riccardo Murgia, Early dark energy is not excluded by current large-scale structure data, Phys. Rev. D **103**, 123542 (2021).

[84] George Alestas, Lavrentios Kazantzidis, and Leandros Perivolaropoulos, $w - M$ phantom transition at $z_t < 0.1$ as a resolution of the Hubble tension, Phys. Rev. D **103**, 083517 (2021).

[85] Andrzej Hryczuk and Krzysztof Jodłowski, Self-interacting dark matter from late decays and the H_0 tension, Phys. Rev. D **102**, 043024 (2020).

[86] Kyriakos Vattis, Savvas M. Koushiappas, and Abraham Loeb, Dark matter decaying in the late Universe can relieve the H0 tension, Phys. Rev. D **99**, 121302 (2019).

[87] Balakrishna S. Haridasu and Matteo Viel, Late-time decaying dark matter: Constraints and implications for the H_0-tension, Mon. Not. R. Astron. Soc. **497**, 1757 (2020).

[88] Steven J. Clark, Kyriakos Vattis, and Savvas M. Koushiappas, Cosmological constraints on late-Universe decaying dark matter as a solution to the H_0 tension, Phys. Rev. D **103**, 043014 (2021).

[89] Ennis Mawas, Lauren Street, Richard Gass, and L. C. R. Wijewardhana, Interacting dark energy axions in light of the Hubble tension, arXiv:2108.13317.

[90] Wenzhong Liu, Luis A. Anchordoqui, Eleonora Di Valentino, Supriya Pan, Yabo Wu, and Weiqiang Yang, Constraints from high-precision measurements of the cosmic microwave background: The case of disintegrating dark matter with Λ or dynamical dark energy, J. Cosmol. Astropart. Phys. 02 (2022) 012.

[91] Eleonora Di Valentino, Alessandro Melchiorri, Olga Mena, and Sunny Vagnozzi, Interacting dark energy in the early 2020s: A promising solution to the H_0 and cosmic shear tensions, Phys. Dark Universe **30**, 100666 (2020).

[92] Eleonora Di Valentino, Alessandro Melchiorri, Olga Mena, and Sunny Vagnozzi, Nonminimal dark sector physics and cosmological tensions, Phys. Rev. D **101**, 063502 (2020).

[93] Weiqiang Yang, Eleonora Di Valentino, Olga Mena, Supriya Pan, and Rafael C. Nunes, All-inclusive interacting dark sector cosmologies, Phys. Rev. D **101**, 083509 (2020).

[94] Eleonora Di Valentino, Alessandro Melchiorri, Olga Mena, Supriya Pan, and Weiqiang Yang, Interacting dark energy in a closed universe, Mon. Not. R. Astron. Soc. **502**, L23 (2021).

[95] Weiqiang Yang, Supriya Pan, Eleonora Di Valentino, Olga Mena, and Alessandro Melchiorri, 2021-H_0 odyssey: Closed, phantom and interacting dark energy cosmologies, J. Cosmol. Astropart. Phys. 10 (2021) 008.

[96] Suresh Kumar and Rafael C. Nunes, Echo of interactions in the dark sector, Phys. Rev. D **96**, 103511 (2017).

[97] Suresh Kumar, Rafael C. Nunes, and Santosh Kumar Yadav, Dark sector interaction: A remedy of the tensions between CMB and LSS data, Eur. Phys. J. C **79**, 576 (2019).

[98] Matteo Lucca and Deanna C. Hooper, Shedding light on dark matter-dark energy interactions, Phys. Rev. D **102**, 123502 (2020).

[99] Weiqiang Yang, Supriya Pan, Rafael C. Nunes, and David F. Mota, Dark calling dark: Interaction in the dark sector in presence of neutrino properties after Planck CMB final release, J. Cosmol. Astropart. Phys. 04 (2020) 008.

[100] Matteo Martinelli, Natalie B. Hogg, Simone Peirone, Marco Bruni, and David Wands, Constraints on the interacting vacuum–geodesic CDM scenario, Mon. Not. R. Astron. Soc. **488**, 3423 (2019).

[101] Adrià Gómez-Valent, Valeria Pettorino, and Luca Amendola, Update on coupled dark energy and the H_0 tension, Phys. Rev. D **101**, 123513 (2020).

[102] Eleonora Di Valentino, Alessandro Melchiorri, and Olga Mena, Can interacting dark energy solve the H_0 tension?, Phys. Rev. D **96**, 043503 (2017).

[103] Suresh Kumar and Rafael C. Nunes, Probing the interaction between dark matter and dark energy in the presence of massive neutrinos, Phys. Rev. D **94**, 123511 (2016).

[104] Weiqiang Yang, Supriya Pan, Eleonora Di Valentino, Rafael C. Nunes, Sunny Vagnozzi, and David F. Mota, Tale of stable interacting dark energy, observational signatures, and the H_0 tension, J. Cosmol. Astropart. Phys. 09 (2018) 019.

[105] Supriya Pan, Weiqiang Yang, and Andronikos Paliathanasis, Non-linear interacting cosmological models after Planck 2018 legacy release and the H_0 tension, Mon. Not. R. Astron. Soc. **493**, 3114 (2020).

[106] Yan-Hong Yao and Xin-He Meng, A new coupled three-form dark energy model and implications for the H_0 tension, Phys. Dark Universe **30**, 100729 (2020).

[107] Yanhong Yao and Xin-He Meng, Relieve the H0 tension with a new coupled generalized three-form dark energy model, Phys. Dark Universe **33**, 100852 (2021).
[108] Supriya Pan, Weiqiang Yang, Eleonora Di Valentino, Emmanuel N. Saridakis, and Subenoy Chakraborty, Interacting scenarios with dynamical dark energy: Observational constraints and alleviation of the H_0 tension, Phys. Rev. D **100**, 103520 (2019).
[109] Weiqiang Yang, Olga Mena, Supriya Pan, and Eleonora Di Valentino, Dark sectors with dynamical coupling, Phys. Rev. D **100**, 083509 (2019).
[110] Supriya Pan, Weiqiang Yang, Chiranjeeb Singha, and Emmanuel N. Saridakis, Observational constraints on sign-changeable interaction models and alleviation of the H_0 tension, Phys. Rev. D **100**, 083539 (2019).
[111] Hassan Amirhashchi and Anil Kumar Yadav, Interacting dark sectors in anisotropic universe: Observational constraints and H_0 tension, arXiv:2001.03775.
[112] Li-Yang Gao, Ze-Wei Zhao, She-Sheng Xue, and Xin Zhang, Relieving the H 0 tension with a new interacting dark energy model, J. Cosmol. Astropart. Phys. 07 (2021) 005.
[113] Matteo Lucca, Multi-interacting dark energy and its cosmological implications, Phys. Rev. D **104**, 083510 (2021).
[114] Daniele Bertacca, Marco Bruni, Oliver F. Piattella, and Davide Pietrobon, Unified Dark Matter scalar field models with fast transition, J. Cosmol. Astropart. Phys. 02 (2011) 018.
[115] Balakrishna S. Haridasu, Matteo Viel, and Nicola Vittorio, Sources of H_0-tension in dark energy scenarios, Phys. Rev. D **103**, 063539 (2021).
[116] N. Menci *et al.*, Constraints on dynamical dark energy models from the abundance of massive galaxies at high redshifts, Astrophys. J. **900**, 108 (2020).
[117] Weiqiang Yang, Supriya Pan, Eleonora Di Valentino, Emmanuel N. Saridakis, and Subenoy Chakraborty, Observational constraints on one-parameter dynamical dark-energy parametrizations and the H_0 tension, Phys. Rev. D **99**, 043543 (2019).
[118] Eleonora Di Valentino, Alessandro Melchiorri, and Joseph Silk, Cosmological constraints in extended parameter space from the Planck 2018 Legacy release, J. Cosmol. Astropart. Phys. 01 (2020) 013.
[119] Eleonora Di Valentino, Ankan Mukherjee, and Anjan A. Sen, Dark energy with phantom crossing and the H_0 tension, Entropy **23**, 404 (2021).
[120] Eleonora Di Valentino, Eric V. Linder, and Alessandro Melchiorri, H_0 ex machina: Vacuum metamorphosis and beyond H_0, Phys. Dark Universe **30**, 100733 (2020).
[121] Weiqiang Yang, Eleonora Di Valentino, Supriya Pan, and Olga Mena, Emergent Dark Energy, neutrinos and cosmological tensions, Phys. Dark Universe **31**, 100762 (2021).
[122] H. B. Benaoum, Weiqiang Yang, Supriya Pan, and Eleonora Di Valentino, Modified emergent dark energy and its astronomical constraints, arXiv:2008.09098.
[123] Weiqiang Yang, Eleonora Di Valentino, Supriya Pan, Yabo Wu, and Jianbo Lu, Dynamical dark energy after Planck CMB final release and H_0 tension, Mon. Not. R. Astron. Soc. **501**, 5845 (2021).
[124] Eleonora Di Valentino, Supriya Pan, Weiqiang Yang, and Luis A. Anchordoqui, Touch of neutrinos on the vacuum metamorphosis: Is the H_0 solution back?, Phys. Rev. D **103**, 123527 (2021).
[125] Weiqiang Yang, Eleonora Di Valentino, Supriya Pan, Arman Shafieloo, and Xiaolei Li, Generalized emergent dark energy model and the Hubble constant tension, Phys. Rev. D **104**, 063521 (2021).
[126] Xiaolei Li and Arman Shafieloo, A simple phenomenological emergent dark energy model can resolve the Hubble tension, Astrophys. J. Lett. **883**, L3 (2019).
[127] Supriya Pan, Weiqiang Yang, Eleonora Di Valentino, Arman Shafieloo, and Subenoy Chakraborty, Reconciling H_0 tension in a six parameter space?, J. Cosmol. Astropart. Phys. 06 (2020) 062.
[128] M. Rezaei, T. Naderi, M. Malekjani, and A. Mehrabi, A Bayesian comparison between ΛCDM and phenomenologically emergent dark energy models, Eur. Phys. J. C **80**, 374 (2020).
[129] Xiaolei Li and Arman Shafieloo, Evidence for emergent dark energy, Astrophys. J. **902**, 58 (2020).
[130] A. Hernández-Almada, Genly Leon, Juan Magaña, Miguel A. García-Aspeitia, and V. Motta, Generalized emergent dark energy: Observational Hubble data constraints and stability analysis, Mon. Not. R. Astron. Soc. **497**, 1590 (2020).
[131] Abdolali Banihashemi, Nima Khosravi, and Amir H. Shirazi, Phase transition in the dark sector as a proposal to lessen cosmological tensions, Phys. Rev. D **101**, 123521 (2020).
[132] Xiaolei Li, Arman Shafieloo, Varun Sahni, and Alexei A. Starobinsky, Revisiting metastable dark energy and tensions in the estimation of cosmological parameters, Astrophys. J. **887**, 153 (2019).
[133] Weiqiang Yang, Eleonora Di Valentino, Supriya Pan, Spyros Basilakos, and Andronikos Paliathanasis, Metastable dark energy models in light of *Planck* 2018 data: Alleviating the H_0 tension, Phys. Rev. D **102**, 063503 (2020).
[134] Abdolali Banihashemi, Nima Khosravi, and Arman Shafieloo, Dark energy as a critical phenomenon: A hint from Hubble tension, J. Cosmol. Astropart. Phys. 06 (2021) 003.
[135] Joan Solà, Adrià Gómez-Valent, and Javier de Cruz Pérez, The H_0 tension in light of vacuum dynamics in the Universe, Phys. Lett. B **774**, 317 (2017).
[136] Ryan E. Keeley, Shahab Joudaki, Manoj Kaplinghat, and David Kirkby, Implications of a transition in the dark energy equation of state for the H_0 and σ_8 tensions, J. Cosmol. Astropart. Phys. 12 (**2019**) 035.
[137] Koushik Dutta, Ruchika, Anirban Roy, Anjan A. Sen, and M. M. Sheikh-Jabbari, Beyond ΛCDM with low and high redshift data: Implications for dark energy, Gen. Relativ. Gravit. **52**, 15 (2020).
[138] W. J. C. da Silva and R. Silva, Growth of matter perturbations in the extended viscous dark energy models, Eur. Phys. J. C **81**, 403 (2021).

[139] Rui-Yun Guo, Jing-Fei Zhang, and Xin Zhang, Can the H_0 tension be resolved in extensions to ΛCDM cosmology?, J. Cosmol. Astropart. Phys. 02 (**2019**) 054.
[140] W. J. C. da Silva and R. Silva, Cosmological perturbations in the tsallis holographic dark energy scenarios, Eur. Phys. J. Plus **136**, 543 (2021).
[141] Eleonora Di Valentino, Ricardo Z. Ferreira, Luca Visinelli, and Ulf Danielsson, Late time transitions in the quintessence field and the H_0 tension, Phys. Dark Universe **26**, 100385 (2019).
[142] Stephen L. Adler, Implications of a frame dependent dark energy for the spacetime metric, cosmography, and effective Hubble constant, Phys. Rev. D **100**, 123503 (2019).
[143] Özgür Akarsu, Suresh Kumar, Emre Özülker, and J. Alberto Vazquez, Relaxing cosmological tensions with a sign switching cosmological constant, Phys. Rev. D **104**, 123512 (2021).
[144] David Benisty and Denitsa Staicova, A preference for dynamical dark energy?, arXiv:2107.14129.
[145] Arindam Mazumdar, Subhendra Mohanty, and Priyank Parashari, Evidence of dark energy in different cosmological observations, Eur. Phys. J. Special Topics **230**, 2055 (2021).
[146] Preeti Shrivastava, A. J. Khan, G. K. Goswami, Anil Kumar Yadav, and J. K. Singh, The simplest parametrization of equation of state parameter in the scalar field Universe, arXiv:2107.05044.
[147] Zhihuan Zhou, Gang Liu, and Lixin Xu, Can phantom transition at $z\tilde{1}$ restore the Cosmic concordance?, Mon. Not. R. Astron. Soc. **511**, 595 (2022).
[148] Chao-Qiang Geng, Yan-Ting Hsu, Jhih-Rong Lu, and Lu Yin, A dark energy model from generalized proca theory, Phys. Dark Universe **32**, 100819 (2021).
[149] Rafael C. Nunes and Eleonora Di Valentino, Dark sector interaction and the supernova absolute magnitude tension, Phys. Rev. D **104**, 063529 (2021).
[150] Aritra Banerjee, Haiying Cai, Lavinia Heisenberg, Eoin Ó. Colgáin, M. M. Sheikh-Jabbari, and Tao Yang, Hubble sinks in the low-redshift swampland, Phys. Rev. D **103**, L081305 (2021).
[151] George Alestas and Leandros Perivolaropoulos, Late-time approaches to the Hubble tension deforming H(z), worsen the growth tension, Mon. Not. R. Astron. Soc. **504**, 3956 (2021).
[152] Giampaolo Benevento, Wayne Hu, and Marco Raveri, Can late dark energy transitions raise the Hubble constant?, Phys. Rev. D **101**, 103517 (2020).
[153] G. Alestas, L. Kazantzidis, and L. Perivolaropoulos, H_0 tension, phantom dark energy, and cosmological parameter degeneracies, Phys. Rev. D **101**, 123516 (2020).
[154] Anastasios Theodoropoulos and Leandros Perivolaropoulos, The Hubble tension, the M crisis of late time H(z) deformation models and the reconstruction of quintessence lagrangians, Universe **7**, 300 (2021).
[155] Valerio Marra and Leandros Perivolaropoulos, Rapid transition of $G_{\rm eff}$ at $z_t \simeq 0.01$ as a solution of the Hubble and growth tensions, Phys. Rev. D **104**, L021303 (2021).
[156] L. Kazantzidis and L. Perivolaropoulos, Hints of a local matter underdensity or modified gravity in the low z pantheon data, Phys. Rev. D **102**, 023520 (2020).
[157] Domenico Sapone, Savvas Nesseris, and Carlos A. P. Bengaly, Is there any measurable redshift dependence on the SN Ia absolute magnitude?, Phys. Dark Universe **32**, 100814 (2021).
[158] L. Kazantzidis, H. Koo, S. Nesseris, L. Perivolaropoulos, and A. Shafieloo, Hints for possible low redshift oscillation around the best-fitting ΛCDM model in the expansion history of the Universe, Mon. Not. R. Astron. Soc. **501**, 3421 (2021).
[159] Maria Giovanna Dainotti, Biagio De Simone, Tiziano Schiavone, Giovanni Montani, Enrico Rinaldi, and Gaetano Lambiase, On the Hubble constant tension in the SNe Ia Pantheon sample, Astrophys. J. **912**, 150 (2021).
[160] George Alestas, Ioannis Antoniou, and Leandros Perivolaropoulos, Hints for a gravitational constant transition in Tully-Fisher data, Universe **7**, 366 (2021).
[161] G. Alestas, L. Perivolaropoulos, and K. Tanidis, Constraining a late time transition of $G_{\rm eff}$ using low-z galaxy survey data, arXiv:2201.05846.
[162] Gilles Esposito-Farese and D. Polarski, Scalar tensor gravity in an accelerating universe, Phys. Rev. D **63**, 063504 (2001).
[163] Amjad Ashoorioon, Carsten van de Bruck, Peter Millington, and Susan Vu, Effect of transitions in the Planck mass during inflation on primordial power spectra, Phys. Rev. D **90**, 103515 (2014).
[164] Licia Verde, Statistical methods in cosmology, Lect. Notes Phys. **800**, 147 (2010).
[165] A. Conley *et al.* (SNLS Collaboration), Supernova constraints and systematic uncertainties from the first 3 years of the supernova legacy survey, Astrophys. J. Suppl. Ser. **192**, 1 (2011).
[166] M. Betoule *et al.* (SDSS Collaboration), Improved cosmological constraints from a joint analysis of the SDSS-II and SNLS supernova samples, Astron. Astrophys. **568**, A22 (2014).
[167] D. M. Scolnic *et al.* (Pan-STARRS1 Collaboration), The complete light-curve sample of spectroscopically confirmed SNe Ia from pan-STARRS1 and cosmological constraints from the combined pantheon sample, Astrophys. J. **859**, 101 (2018).
[168] Stephen M. Feeney, Daniel J. Mortlock, and Niccolò Dalmasso, Clarifying the Hubble constant tension with a Bayesian hierarchical model of the local distance ladder, Mon. Not. R. Astron. Soc. **476**, 3861 (2018).
[169] E. Macaulay *et al.* (DES Collaboration), First cosmological results using type ia supernovae from the dark energy survey: Measurement of the Hubble constant, Mon. Not. R. Astron. Soc. **486**, 2184 (2019).
[170] David Camarena and Valerio Marra, On the use of the local prior on the absolute magnitude of Type Ia supernovae in cosmological inference, Mon. Not. R. Astron. Soc. **504**, 5164 (2021).
[171] George Efstathiou, To H0 or not to H0?, Mon. Not. R. Astron. Soc. **505**, 3866 (2021).
[172] Leandros Perivolaropoulos and Foteini Skara, Hubble tension or a transition of the Cepheid SnIa calibrator parameters?, Phys. Rev. D **104**, 123511 (2021).
[173] Edvard Mortsell, Ariel Goobar, Joel Johansson, and Suhail Dhawan, The Hubble tension bites the dust: Sensitivity of

the Hubble constant determination to cepheid color calibration, arXiv:2105.11461.
[174] David Camarena and Valerio Marra, Local determination of the Hubble constant and the deceleration parameter, Phys. Rev. Research **2**, 013028 (2020).
[175] Varun Sahni and Alexei Starobinsky, Reconstructing dark energy, Int. J. Mod. Phys. D **15**, 2105 (2006).
[176] N. Aghanim *et al.* (Planck Collaboration), Planck 2018 results. VI. Cosmological parameters, Astron. Astrophys. **641**, A6 (2020).
[177] N. Aghanim *et al.* (Planck Collaboration), Planck 2018 results. V. CMB power spectra and likelihoods, Astron. Astrophys. **641**, A5 (2020).
[178] N. Aghanim *et al.* (Planck Collaboration), Planck 2018 results. VIII. Gravitational lensing, Astron. Astrophys. **641**, A8 (2020).
[179] Shadab Alam *et al.* (BOSS Collaboration), The clustering of galaxies in the completed SDSS-III baryon oscillation spectroscopic survey: Cosmological analysis of the DR12 galaxy sample, Mon. Not. R. Astron. Soc. **470**, 2617 (2017).
[180] Florian Beutler, Chris Blake, Matthew Colless, D.Heath Jones, Lister Staveley-Smith, Lachlan Campbell, Quentin Parker, Will Saunders, and Fred Watson, The 6dF galaxy survey: Baryon acoustic oscillations and the local Hubble constant, Mon. Not. R. Astron. Soc. **416**, 3017 (2011).
[181] Ashley J. Ross, Lado Samushia, Cullan Howlett, Will J. Percival, Angela Burden, and Marc Manera, The clustering of the SDSS DR7 main galaxy sample—I. A 4 per cent distance measure at $z = 0.15$, Mon. Not. R. Astron. Soc. **449**, 835 (2015).
[182] Michael Blomqvist *et al.*, Baryon acoustic oscillations from the cross-correlation of Lyα absorption and quasars in eBOSS DR14, Astron. Astrophys. **629**, A86 (2019).
[183] Victoria de Sainte Agathe *et al.*, Baryon acoustic oscillations at z = 2.34 from the correlations of Lyα absorption in eBOSS DR14, Astron. Astrophys. **629**, A85 (2019).
[184] D. M. Scolnic *et al.*, The complete light-curve sample of spectroscopically confirmed SNe Ia from Pan-STARRS1 and cosmological constraints from the combined pantheon sample, Astrophys. J. **859**, 101 (2018).
[185] Bryan Sagredo, Savvas Nesseris, and Domenico Sapone, Internal robustness of growth rate data, Phys. Rev. D **98**, 083543 (2018).
[186] Rubén Arjona, Juan García-Bellido, and Savvas Nesseris, Cosmological constraints on nonadiabatic dark energy perturbations, Phys. Rev. D **102**, 103526 (2020).
[187] Thejs Brinckmann and Julien Lesgourgues, MontePython 3: Boosted MCMC sampler and other features, Phys. Dark Universe **24**, 100260 (2019).
[188] Benjamin Audren, Julien Lesgourgues, Karim Benabed, and Simon Prunet, Conservative Constraints on Early Cosmology: An illustration of the Monte Python cosmological parameter inference code, J. Cosmol. Astropart. Phys. 02 (2013) 001.
[189] Diego Blas, Julien Lesgourgues, and Thomas Tram, The cosmic linear anisotropy solving system (class). Part II: Approximation schemes, J. Cosmol. Astropart. Phys. 07 (2011) 034.
[190] Adam G. Riess *et al.*, A comprehensive measurement of the local value of the Hubble constant with 1 km/s/Mpc uncertainty from the Hubble space telescope and the SH0ES team, arXiv:2112.04510.
[191] S. Dhawan, D. Brout, D. Scolnic, A. Goobar, A. G. Riess, and V. Miranda, Cosmological model insensitivity of local H_0 from the cepheid distance ladder, Astrophys. J. **894**, 54 (2020).
[192] David Camarena and Valerio Marra, A new method to build the (inverse) distance ladder, Mon. Not. R. Astron. Soc. **495**, 2630 (2020).
[193] Michel Chevallier and David Polarski, Accelerating universes with scaling dark matter, Int. J. Mod. Phys. D **10**, 213 (2001).
[194] Eric V. Linder, Exploring the Expansion History of the Universe, Phys. Rev. Lett. **90**, 091301 (2003).
[195] H. Akaike, A new look at the statistical model identification, IEEE Trans. Autom. Control **19**, 716 (1974).
[196] Savvas Nesseris and Juan Garcia-Bellido, Is the Jeffreys' scale a reliable tool for Bayesian model comparison in cosmology?, J. Cosmol. Astropart. Phys. 08 (2013) 036.
[197] Alan Heavens, Yabebal Fantaye, Arrykrishna Mootoovaloo, Hans Eggers, Zafiirah Hosenie, Steve Kroon, and Elena Sellentin, Marginal likelihoods from Monte Carlo Markov Chains, arXiv:1704.03472.
[198] Prasanta Chandra Mahalanobis, *On the Generalized Distance in Statistics* (National Institute of Science of India, Calcuta, 1936).
[199] Roberto Trotta, Bayes in the sky: Bayesian inference and model selection in cosmology, Contemp. Phys. **49**, 71 (2008).
[200] James Alvey, Nashwan Sabti, Miguel Escudero, and Malcolm Fairbairn, Improved BBN constraints on the variation of the gravitational constant, Eur. Phys. J. C **80**, 148 (2020).
[201] Enrique Gaztanaga, Anna Cabre, and Lam Hui, Clustering of luminous red galaxies IV: Baryon acoustic peak in the line-of-sight direction and a direct measurement of H(z), Mon. Not. R. Astron. Soc. **399**, 1663 (2009).
[202] Jean-Philippe Uzan, The fundamental constants and their variation: Observational status and theoretical motivations, Rev. Mod. Phys. **75**, 403 (2003).
[203] Leandros Perivolaropoulos, Is the Hubble crisis connected with the extinction of dinosaurs?, arXiv:2201.08997.
[204] Eugene M. Shoemaker, Impact cratering through geologic time, J. R. Astron. Soc. Can. **92**, 297 (1998).
[205] T. Gehrels, *Hazards Due to Comets and Asteroids* (University of Arizona Press, 1995).
[206] Alfred S. McEwen, Jeffrey M. Moore, and Eugene M. Shoemaker, The phanerozoic impact cratering rate: Evidence from the farside of the moon, J. Geophys. Res. **102**, 9231 (1997).
[207] Jennifer A. Grier, Alfred S. McEwen, Paul G. Lucey, Moses Milazzo, and Robert G. Strom, Optical maturity of ejecta from large rayed lunar craters, J. Geophys. Res. **106**, 32847 (2001).
[208] S. Ward and S. Day, Terrestrial crater counts: Evidence of a two to four-fold increase in bolide flux at

125 ma (2007), https://websites.pmc.ucsc.edu/~ward/papers/crater-counts(v2.4).pdf.
[209] Mario Livio and Paolo Mazzali, On the progenitors of type Ia supernovae, Phys. Rep. **736**, 1 (2018).
[210] Saurabh W. Jha, Kate Maguire, and Mark Sullivan, Observational properties of thermonuclear supernovae, Nat. Astron. **3**, 706 (2019).
[211] A. Flörs, J. Spyromilio, S. Taubenberger, S. Blondin, R. Cartier, B. Leibundgut, L. Dessart, S. Dhawan, and W. Hillebrandt, Sub-Chandrasekhar progenitors favoured for type Ia supernovae: Evidence from late-time spectroscopy, Mon. Not. R. Astron. Soc. **491**, 2902 (2020).
[212] https://github.com/lkazantzi/H0_Model_Comparison.